CDDpress

www.nature.com/cddis

ARTICLE OPEN

BAP1 dysregulation impairs trophoblast differentiation and contributes to placental dysfunction in preeclampsia

Paula Doria-Borrell[1,2], Ana Ferrero-Micó[1,2], Sergio Navarro-Serna[2], Maravillas Mellado-López[2], Johanna Grinat[1], Ciara N Murphy[3,4], Lina Youssef[5], Fàtima Crispi[5,6], Tu'uhevaha J Kaitu'u-Lino[3,4] and Vicente Pérez-García[1,2]✉

© The Author(s) 2026

Preeclampsia, a life-threatening hypertensive disorder of pregnancy, is a leading cause of maternal and perinatal morbidity and mortality. Its early-onset form (EO-PE), requiring delivery before 34 weeks of gestation, is particularly severe and closely linked to defective trophoblast differentiation. Here, we identify BRCA1-associated protein 1 (BAP1) and its cofactors ASXL2 and ASXL3 as upregulated in EO-PE placentas. Enforced BAP1 expression in human trophoblast stem cells reinforced epithelial identity, enhanced adhesion, and impaired both extravillous trophoblast differentiation and syncytiotrophoblast formation. Integrated transcriptomic and proteomic analyses revealed suppression of lineage-specific pathways alongside maintenance of progenitor-like and pro-inflammatory signatures. In trophoblast organoids, an excess of BAP1 disrupted syncytial maturation and induced interferon-driven pathways overlapping with EO-PE transcriptomes. Together, these findings establish BAP1 as a key regulator of human trophoblast differentiation and implicate its dysregulation in the pathogenesis of EO-PE, providing mechanistic insight into the cellular basis of placental dysfunction.

Cell Death and Disease (2026)17:410 ; https://doi.org/10.1038/s41419-026-08650-z

INTRODUCTION

The human placenta is a transient yet essential organ that supports fetal development by mediating maternal–fetal exchange and regulating immune and endocrine interactions throughout gestation. Its architecture and function are established early in pregnancy through the expansion and differentiation of cytotrophoblasts (CTBs), which give rise to syncytiotrophoblasts (STBs) and extravillous trophoblasts (EVTs). STBs form the outer multinucleated layer of the chorionic villi, mediating nutrient and gas exchange, while EVTs migrate into the maternal decidua to remodel uterine spiral arteries and ensure adequate blood flow to the developing fetus. The differentiation of CTBs into these specialized trophoblast lineages is therefore fundamental for normal placental development and function [1–3]. Early studies using isolated primary CTBs and first-trimester placental explants yielded valuable insights into human trophoblast biology, including the processes of syncytial fusion and EVT invasion. Although informative, these models are restricted by limited tissue availability, intrinsic cellular heterogeneity, and their inability to sustain proliferative trophoblast populations in culture. As a result, they provide only a narrow window into how trophoblast progenitor states are defined, stabilized, or perturbed during early placental development [4]. A major advance came with the derivation of human trophoblast stem cells (hTSCs) from blastocysts and first-trimester villi, which established a renewable source of trophoblast progenitors capable of differentiating into both major placental lineages [5]. The subsequent development of trophoblast organoids from first-trimester tissue further addressed the need for physiologically relevant in vitro systems [6, 7]. These three-dimensional structures recreate core architectural and functional hallmarks of the trophoblast epithelium, including lineage diversification, spatial organization, and robust endocrine activity.

Together, hTSC and trophoblast organoid platforms have transformed experimental access to human-specific mechanisms governing trophoblast fate. Their genetic tractability and lineage fidelity now allow systematic exploration of how molecular regulators control the balance between self-renewal, differentiation, and programmed cell death. These models, therefore, constitute an essential framework for interpreting how dysregulated trophoblast programs contribute to placental dysfunction and pregnancy disorders.

Defective trophoblast differentiation is a hallmark of placental disorders, most notably preeclampsia (PE), a hypertensive pregnancy complication with major maternal and perinatal morbidity [8, 9]. PE is increasingly recognized as a heterogeneous disorder with distinct early- and late-onset subtypes [10]. Early-onset PE (EO-PE) occurs before 34 weeks of gestation and is primarily driven by defective placentation, including shallow EVT invasion, impaired spiral artery remodeling, and diminished syncytialization [11–13]. EO-PE placentas also exhibit heightened oxidative stress and activation of the unfolded protein response

[1]Centro de Biología Molecular Severo Ochoa, Madrid, Spain. [2]Centro de Investigación Príncipe Felipe, Valencia, Spain. [3]The Department of Obstetrics, Gynaecology and Newborn Health/Mercy Hospital for Women, University of Melbourne, Heidelberg, VIC, Australia. [4]Mercy Perinatal, Mercy Hospital for Women, Heidelberg, VIC, Australia. [5]BCNatal - Barcelona Center for Maternal-Fetal and Neonatal Medicine, Hospital Sant Joan de Déu and Hospital Clínic, University of Barcelona, Barcelona, Spain. [6]Centre for Biomedical Research on Rare Diseases (CIBER-ER), Madrid, Spain. ✉email: vperez@cbm.csic.es

Edited by Professor Massimiliano Agostini

Received: 6 August 2025 Revised: 19 February 2026 Accepted: 11 March 2026
Published online: 26 March 2026

(UPR), which suppresses non-essential protein synthesis in an attempt to restore endoplasmic reticulum (ER) homeostasis [14]. Consistent with this heightened stress, shedding of syncytiotrophoblast-derived micro- and nanovesicles, including exosomes carrying regulatory microRNAs, is markedly increased in EO-PE compared to both healthy pregnancies and late-onset disease [15–18]. In contrast, late-onset PE (LO-PE), which manifests after 34 weeks, is thought to reflect a mismatch between normal placental aging and the increasing metabolic demands of the fetus in the context of maternal predisposition to cardiovascular or metabolic disease [10]. LO-PE is frequently associated with maternal inflammation, elevated BMI, and higher arterial pressure, and although placental dysfunction is present, it is generally less severe than in EO-PE [19]. Despite these advances, the regulators that govern trophoblast lineage decisions in EO-PE and differentiate it from the largely maternal-driven pathology of LO-PE remain unclear.

Our previous work in mice identified BRCA1-associated protein 1 (BAP1) as a key regulator of placentation [20]. BAP1 functions as the catalytic subunit of the Polycomb Repressive-DUB (PR-DUB) complex by interacting with additional sex comb-like (ASXL1/2/3) proteins to deubiquitinate histone H2A at lysine 119 (H2AK119), maintaining its spatial distribution and exerting its tumour suppressor activity [21–23]. Mouse models deficient in Bap1 exhibit severe placental abnormalities and midgestational lethality [20]. In both murine and human placentas, BAP1 is highly expressed in proliferative CTBs and downregulated during differentiation into EVTs and STBs, suggesting a conserved role in lineage regulation [24].

Here, we dissect the role of BAP1 in human trophoblast development using CRISPR/Cas9 knockout technology and genetic overexpression in hTSCs. We show that BAP1 is upregulated in EO-PE placentas, supporting its pathological relevance. We demonstrate that high BAP1 expression sustains epithelial features, impedes differentiation into both EVTs and STBs, and mimics molecular signatures of EO-PE. Our findings highlight proper BAP1 modulation as a critical step in trophoblast differentiation, with direct implications for the etiology of preeclampsia.

MATERIAL AND METHODS

Human samples

Melbourne cohort. Details on the number and characteristics of the patients and control subjects are provided in Supplementary File 1. The study was approved by the Mercy Health Human Research Ethics Committee (R11/34), and written informed consent was obtained from all participants prior to sample collection. Placental tissue samples were collected in Melbourne within 30 min of delivery and snap-frozen at −80 °C for subsequent RNA extraction. Total mRNA was extracted and reverse-transcribed into cDNA using the High-Capacity cDNA Reverse Transcription Kit (Applied Biosystems, Life Technologies, Carlsbad, CA) with 400 ng of input mRNA, according to the manufacturer's instructions. The thermal cycling conditions were: 25 °C for 10 min, 37 °C for 60 min, and 85 °C for 5 min. cDNA was stored at −20 °C. Quantitative PCR was performed using a CFX384 real-time PCR system (Bio-Rad) and Fast SYBR Master Mix (Thermo Fisher Scientific, Scoresby, Australia). The cycling conditions were: 95 °C for 20 s, followed by 40 cycles of 95 °C for 1 s and 60 °C for 20 s, with a melt curve from 65 °C to 95 °C in 0.5 °C increments every 5 s.

Barcelona cohort

Sixteen singleton pregnancies were prospectively recruited at the Department of Maternal-Fetal Medicine, Hospital Clinic (Barcelona, Spain) between 2017 and 2021. The study population comprised pregnancies complicated by preeclampsia ($n = 8$) and normotensive pregnancies ($n = 8$) who were selected from our general population to be matched with cases by baseline maternal characteristics. Preeclampsia cases were consecutively recruited, and those patients with collected placental samples were selected for this study. The cohort included normotensive pregnancies ($n = 8$) and cases of preeclampsia ($n = 8$), defined as systolic blood pressure >140 mmHg and/or diastolic blood pressure >90 mmHg on two separate occasions (≥ 4 h apart) after 20 weeks of gestation, accompanied by proteinuria (> 300 mg/24 h or protein/creatinine ratio >300 mg/g) or signs of end-organ dysfunction [25]. Early-onset preeclampsia was defined as requiring delivery before 34 weeks' gestation; late-onset cases were delivered at or after 34 weeks. Controls were matched for baseline characteristics, including several preterm deliveries due to spontaneous labor or non-hypertensive indications. Exclusion criteria included fetal anomalies, chromosomal abnormalities, and intrauterine infections. Gestational age was determined by first-trimester crown-rump length. Ethics approval was granted by the Hospital Clinic Ethics Committee (HCB-2016-0830), and written informed consent was obtained from all participants.

Placental tissues were collected at delivery, snap-frozen, and stored at −80 °C. Samples were handled on dry ice. Tissue exceeding ~30 mg was trimmed on a pre-chilled P60 plate and transferred to matrix A-tubes using a 21 G needle. Samples were homogenized using the FastPrep-24 5 G system (MP Biomedicals) in 300 µL of TRIzol or Triplex + CI. Four homogenization cycles were performed, with the rotor placed on ice between runs. Samples were centrifuged at 14,000 × *g* for 10 min at 4 °C. The supernatant was transferred to fresh tubes. For viscous samples, 200 µL of additional TRIzol was added, followed by vortexing and repeated centrifugation under identical conditions. Final supernatants were stored at −80 °C.

For protein extraction, tissues were homogenized in RIPA buffer (1X) supplemented with protease/phosphatase inhibitors (CI) and PMSF. Homogenization was conducted using the same FastPrep-24 protocol as above. After centrifugation (14,000 × *g*, 10 min, 4 °C), the supernatant was collected, sonicated for 5 min, and quantified. Proteins were resolved on 7% SDS-PAGE gels and transferred at 290 mA for 90 min. Standard western blot procedures were followed for membrane blocking and antibody incubation.

An alternative extraction method using an Ultraturrax homogenizer (Polytron) was employed for optimization. Placental fragments were homogenized in 350 µL of RIPA + CI + PMSF on ice with two 20-second pulses separated by a 30-s cooling interval. The homogenate was centrifuged (maximum speed, 10 min, 4 °C), and the supernatant was processed for protein quantification and western blotting as described above.

Culture and differentiation of human trophoblast cell lines

BTS11 blastocyst-derived hTSCs were obtained from Professor Takahiro Arima and cultured following the protocol described by Okae et al. (2018), with an increased concentration of CHIR99021 [5].In summary, hTSCs were plated at a density of 0.5–1 × 10^6 cells per well on six-well plates coated with 5 mg/mL collagen IV (Cultrex 3410-010-02). The cells were maintained in 2 mL of TS medium, which consisted of DMEM/F12 (Gibco 31331-028) supplemented with 0.3% BSA (Sigma A8412), 1% ITS-X supplement (Gibco 51500-056), 0.1 mM 2-mercaptoethanol (Gibco 31350), 0.2% FBS (Gibco 10270), 100 µg/mL Primocin (Invivogen ant-pm-1), 1.5 µg/mL L-ascorbic acid (Sigma A8960), 50 ng/mL EGF (Peprotech AF-100-15), 4 µM CHIR99021 (Tocris 4423), 0.5 µM A83-01 (Systems Biosciences ZRD-A8-02), 1 µM SB431542 (Tocris 1614), 0.8 mM VPA (Sigma P4543), and 5 µM Rock Inhibitor Y27632 (Millipore 688000). Cultures were maintained at 37 °C with 5% CO_2, and the medium was replaced every two days. For passaging, cells were detached using TrypLE (Gibco 12604-013) for 10–15 min at 37 °C.

For differentiation into extravillous trophoblasts (EVTs), the method followed was based on the protocol described in [24]. Briefly, hTSCs at 80% confluence were detached using TrypLE and resuspended as single cells. A total of 0.75 × 10^5 cells were plated onto six-well plates coated with 1 µg/mL collagen IV and cultured in 2 mL of EVT medium. This medium consisted of DMEM/F12 supplemented with 0.1 mM 2-mercaptoethanol, 0.5% penicillin–streptomycin, 0.3% BSA, 1% ITS-X supplement, 100 ng/mL NRG1, 7.5 µM A83-01, 2.5 µM Y27632, and 4% KSR. Additionally, Matrigel was included at a final concentration of 2%. On day 3, the medium was changed to EVT medium without NRG1, with Matrigel adjusted to 0.5%. On day 6, the medium was refreshed again, this time omitting both NRG1 and KSR while keeping Matrigel at 0.5%. The differentiation process was assessed on day 8.

To induce syncytiotrophoblast (STB) differentiation, hTSCs at approximately 80% confluence were dissociated into single cells using TrypLE. A total of 1.5 × 10^5 cells were then seeded onto a fresh six-well plate pre-coated with 3 µg/mL collagen IV. The cells were cultured in STB

differentiation medium, as outlined by Okae et al. (2018), which included DMEM/F12 GlutaMAX (Gibco 31331-028) with 0.1 mM 2-mercaptoethanol (Gibco 31350), 4% KSR, 0.3% BSA (Sigma A8412), 1% ITS-X supplement (Gibco 51500-056), 2.5 µM Y27632 (Millipore 688000), 2 µM forskolin (Sigma 93049), and 0.5% Primocin (Invivogen ant-pm-1). The medium was refreshed on day 2, and analyses were performed on day 4.

Organoid culture

The transition from 2D cultures to 3D trophoblast organoids was carried out by seeding a single-cell suspension onto 25 µL Matrigel droplets in 48-well plates. The culturing process followed the established protocol described in [26]. After incubating the Matrigel droplets with organoids for 10 min at 37 °C, cultures were overlaid with trophoblast organoid medium (TOM). This medium comprised Advanced DMEM/F12 (Thermo Fisher Scientific), N2 supplement (Thermo Fisher Scientific, 17502048), B27 supplement without vitamin A (Thermo Fisher Scientific, 12587010; used as per the manufacturer's instructions), 100 µg/mL Primocin (InvivoGen, ant-pm), 1.25 mM N-acetyl-L-cysteine (Sigma-Aldrich, A9165), 2 mM L-glutamine (Sigma-Aldrich, 25030024), 50 ng/mL recombinant human EGF (Peprotech, AF10015), 1.5 µM CHIR99021 (Tocris, 4423), 80 ng/mL recombinant human R-spondin-1 (R&D Systems, 4645-RS-01M/CF), 100 ng/mL recombinant human FGF-2 (Peprotech, 100-18B), 50 ng/mL recombinant human HGF (Peprotech, 100-39), 500 nM A83-01 (Tocris, 2939), 2.5 µM prostaglandin E2 (Sigma-Aldrich, P0409), and 2 µM Y-27632 (Millipore, 688000).

To pass the organoids, Matrigel droplets were collected into 1.5 mL tubes and mechanically dissociated through repeated pipetting (~400 times) until the organoids were broken down. The resulting organoid suspension was then washed with Advanced DMEM/F12 and reseeded into fresh Matrigel droplets. For pellet collection, organoid droplets were transferred into 1.5 mL tubes containing Cell Recovery Solution and incubated for 30 min at 4 °C. After washing with PBS, organoids were either analyzed immediately or stored at −80 °C for later use.

CRISPR-Cas9-mediated knockdown in hTSCs

For CRISPR/Cas9-mediated knockdown of BAP1, sgRNA oligonucleotides (Integrated DNA Technologies) were designed to target regions upstream and downstream of BAP1 exon 4 using http://crispor.tefor.net/, as described in Doria-Borrell et al. (2024). A total of four sgRNAs were designed: two upstream (1 A and 1B) and two downstream (2 A and 2B) of exon 4. The sgRNA sequences were as follows: 1 A, 5′-TTTGCACTGCGTCATCACTC-3′; 1B, 5′-TGAGTGATGACGCAGTGCAA-3′; 2 A, 5′-CAGAGCAGGTCAGTCATATC-3′; and 2B, 5′-AGTTCAGTTCGTTCTGCCAG-3′.

Each sgRNA sequence was cloned into either pSpCas9(BB)-2A-GFP (PX458; Addgene plasmid #48138) or pSpCas9(BB)-2A-Puro V2.0 (PX459; Addgene plasmid #62988). Human trophoblast stem cells (hTSCs) were transfected with plasmid combinations of (1A–puromycin + 2A–GFP) or (1A–puromycin + 2B–GFP) using Opti-MEM (Thermo Fisher Scientific) and Lipofectamine 2000 reagent according to the manufacturer's instructions (Thermo Fisher, 11668019). Forty-eight hours after transfection, GFP^+ cells were sorted using a FACSAria II system and replated onto 6-well plates according to cell number. Then, cells were treated with 1 µg/mL puromycin for 3 days.

Lentivirus over-expression in hTSCs

BTS11 cells were transduced with lentiviral particles of pLV[Exp]-EGFP:T2A:Puro-CMV > ORF_Empty (Control) or (pLV [Exp]-Puro-CMV > EGFP:hBAP1[NM_004656.4] or pLV[Exp]-EGFP/Puro-EF1A > hBAP1[NM_004656.4] to overexpress BAP1. In both cases, the lentiviral particles were packaged by VectorBuilder. Cells were transduced with the lentivirus supplemented with 8 µg/mL polybrene (Millipore, TR-1003-G) for 24 h. After 48 h, cells were selected by sorting and collecting all GFP+ cells in one P48 cell plate. After cell expansion, we selected again by adding 1 µg/mL puromycin to the medium for 7 days.

Proliferation assay

Trophoblast cells (150.000 cells/well) were seeded in a 6-well plate pre-coated with 5 mg/mL Col IV (Cultrex 3410-010-02). Cells were collected every 24 h using TrypLE (Gibco 12604-013) for 10 to 15 min at 37 °C, and viable cells were counted using trypan blue exclusion on a LUNA II Automated Cell Counter (Logos Biosystems) according to the manufacturer's instructions. Data was analysed using two-way ANOVA with Sidák's multiple comparisons test (p-value < 0.05) using GraphPad Prism 9.

Cell adhesion assay

The adhesion capacity of control, BAP1 knockdown (BAP1-KD), and BAP1-overexpressing (BAP1-OE) human trophoblast stem cells (hTSCs) was assessed using the Vybrant Cell Adhesion Assay Kit (Thermo Fisher Scientific, V13181), following the manufacturer's instructions and as previously described [27].

Briefly, a 96-well tissue culture plate was coated with 5 mg/mL collagen IV (Cultrex, 3410-010-02). Cells were resuspended in DMEM/F12 GlutaMAX (Gibco, 31331-028) containing 5 µL of Vybrant labeling reagent and incubated for 30 min at 37 °C. Labeled cells were washed with phosphate-buffered saline (PBS; Cytiva, SH30028.02) and resuspended in hTSC complete medium.

A total of 5×10^4 labeled cells were seeded per well into four replicate collagen-coated wells and three uncoated wells (negative control) and allowed to adhere for 4 h at 37 °C. Following incubation, wells were washed three times with PBS to remove non-adherent cells, and fluorescence was measured at 517 nm using a PHERAstar FS plate reader (BMG Labtech). Data were analyzed using a two-tailed Student's t test, with statistical significance set at $p < 0.05$ (GraphPad Prism v9).

Gelatin zymography

Matrix metalloproteinase (MMP) activity in hTSCs and differentiated extravillous trophoblasts (EVTs) was assessed by gelatin zymography. hTSCs were cultured to high confluency, and EVTs were collected on day 7 of differentiation. At this stage, cells were cultured in serum-free medium for 24 h. Conditioned media were then collected, and total protein concentrations were determined using a calibration curve.

For each sample, 10 µL of conditioned medium was mixed with 5× non-reducing sample buffer (4% SDS, 20% glycerol, 0.01% bromophenol blue, 125 mM Tris-HCl, pH 6.8) and loaded onto SDS–polyacrylamide gels (7.5% separating gel and 4% stacking gel) containing gelatin as a substrate. Electrophoresis was carried out at 100 V until the protein front migrated into the separating gel, followed by a voltage increase to 140 V until completion.

Gels were washed twice for 30 min in washing buffer (2.5% Triton X-100, 50 mM Tris-HCl, pH 7.5, 5 mM $CaCl_2$, 1 µM $ZnCl_2$) at room temperature with agitation to remove SDS and restore enzyme activity. Gels were then incubated for 5–10 min in incubation buffer (1% Triton X-100, 50 mM Tris-HCl, 5 mM $CaCl_2$, 1 µM $ZnCl_2$) at 37 °C, followed by a 24-h incubation in fresh incubation buffer at 37 °C.

Following incubation, gels were stained in 40% methanol, 10% acetic acid, and 0.5 g/L Coomassie Brilliant Blue R-250 for 30–60 min at room temperature with agitation, then destained in 40% methanol and 10% acetic acid until clear bands of gelatinolytic activity were visible. Gels were imaged using the ImageQuant system, and MMP activity was quantified by densitometry using ImageJ software (NIH).

RNA extraction and RT-qPCR

Total RNA was extracted using the RNeasy mini-Kit and RNase-free DNase (QIAGEN 74106). First, cDNA was synthesized from total RNA using PrimeScript RT Master Mix (Takara Bio RR036A), and real-time PCR reaction was done with the TB Green Premix Ex Taq (Takara Bio RR420L) on a LC480 II thermocycler in a 384 plate. The geometric mean of *YWHAZ* and *TBP* was used as housekeeping genes. Full list of primers can be consulted in Supplementary File 2. For statistical analysis, a two-way ANOVA with Tukey's multiple comparisons test (p-value < 0.05) were performed to calculate statistical significance of expression differences using GraphPad Prism 9.

Western blot

Samples collected for Western blot analysis were lysed in RIPA buffer (50 mM tris-HCl, 150 mM NaCl, IGEPAL CA-630, 0.75% sodium deoxycholate, 0.1% SDS), containing a protease inhibitor cocktail (Sigma P2714), and incubated at 4 °C for 1 h, followed by centrifugation (9300 × g, 10 min). Western blotting was performed as in [28]. Blots were probe against the antibodies anti-SDC1 1:1000 (Abcam, ab128936), anti-HSP90 1:5000 (Cell Signaling, 4877S), anti-TUBULIN (1:5000, Abcam, ab6160), anti-BAP1 1:1000 (Cell signaling, 1318S), anti-ASXL1 1:1000 (Abnova, H00171023-M05), anti-ASXL2 1:1000 (Bethyl, A302-037A), anti-ASXL3 1:500 (MyBioSource, MBS5401046), anti-HLA-G 1:1000 (Biorad, MCA2043), anti-ACTIN 1:5000 (Biorad, ab6276), followed by horseradish peroxidase-conjugated secondary antibodies anti-rabbit (Bio-Rad 170–6515) and anti-mouse (Bio-Rad 170–6516, all 1:3000) (Supplementary file Original data). Detection was carried out with enhanced chemiluminescence reaction (GE Healthcare

RPN2209) on X-ray films. The intensity of the bands was quantified using ImageJ software.

Immunofluorescence staining

Cells were fixed with 4% paraformaldehyde (PFA) in phosphate-buffered saline (PBS) for 10 min and permeabilized with PBS, 0.3% Triton X-100 for 10 min. Blocking was carried out with PBS, 0.1% Tween 20, 1% BSA (PBT/BSA) for 30 min, followed by antibody incubation for 60 min. Primary antibodies and dilutions (in PBT/BSA) were E-cadherin (CDH1) 1:100 (BD Biosciences, 610181)), CGb 1:100 (Abcam, ab9582), SDC1) 1:100 (Abcam, AB128936), and DESMOPLAKIN 1:100 (Abcam, ab71690), followed by secondary antibodies Alexa Fluor 568 or 647 (Thermo Fisher Scientific) diluted 1:400 in blocking buffer.

Organoid staining was performed following a modification of the protocol previously described [24]. Briefly, Matrigel was removed from organoids using Cell Recovery Solution (Corning) and fixed for 1 h in 4% PFA at RT. After three washes (15 min) with PBS supplemented with 3 mg/ml poly-vinylpyrrolidone (Sigma, P0930), organoids were permeabilized with PBS containing 5% DMSO, 0.5% Triton X-100, 0.1% BSA, 0.01% Tween 20 for 3 h. Then, organoids were blocked overnight at 4 °C in permeabilization buffer, containing 2% Fetal Bovine Serum. Organoids were incubated overnight at 4 °C with antibodies against CDH1 at 1:100 (BD Biosciences, 610181), CGβ at 1:100 (Abcam, ab9582), and SDC1 at 1:100 (Abcam, AB128936), in blocking buffer, followed by three washes in blocking buffer for 1 h. Then, organoids were incubated overnight with secondary Alexa Fluor 568 or 647 (Thermo Fisher Scientific) antibodies diluted 1:400 in blocking buffer. Lastly, organoids were washed three times for 1 h in blocking buffer, and nuclei were counter-stained with DAPI for 10 min. Organoids were mounted in Vectashield (Vector Laboratories, H-1000), surrounded by spacer drops of vaseline for the coverslip, to immobilize the organoids. Images were taken with an LSM900 Vertical confocal microscope.

Analysis of organoid perimeter

Measurements of total organoid and syncytiotrophoblast perimeters were performed using bright-field images acquired with an EVOS microscope. Image analysis was conducted in ImageJ, where the perimeter of each organoid was manually outlined and measured. To ensure accuracy and account for variability, each organoid was measured three times, and the mean perimeter was calculated. Statistical comparison was Student's two-tailed t-tests, performed using GraphPad Prism (v9.4.1). Statistical significance was set at $p < 0.05$.

RNA-seq sample preparation

RNA samples were extracted using the RNeasy mini-Kit and RNase-free DNase (QIAGEN 74106). QC, library preparation, sequencing, and mapping were performed by Novogene using an Illumina Novaseq 6000 with 150 bp paired-end reads.

Proteomics LC-MS/MS

Proteomic analysis was conducted by liquid chromatography–tandem mass spectrometry (LC–MS/MS) at the Proteomics Service of the Servicio Central de Soporte a la Investigación Experimental (University of Valencia). Protein samples were collected in RIPA buffer under the same conditions used for Western blot analysis, and 10 µg of total protein was used per sample.

Sample preparation followed the SP3 protocol for detergent removal and sample clean-up prior to enzymatic digestion with trypsin, as described by Moggridge et al. and Müller et al. with minor modifications [29, 30]. Following digestion, 2 µL of each sample were diluted to a final volume of 20 µL with 0.1% formic acid and loaded onto Evotip Pure tips (EvoSep) according to the manufacturer's instructions. Peptide identification was carried out using MSFragger (via FragPipe) against the SwissProt human protein database. Protein quantification and differential expression analysis were performed using the default DIA-NN workflow.

Bioinformatics analysis

RNA-seq data were quantified using the SeqMonk RNA-seq quantitation pipeline (http://www.bioinformatics.babraham.ac.uk) and normalized by total read count, expressed as reads per million mapped reads. Differential expression analysis was carried out using DESeq2, applying a cutoff of $\log_2$ fold change ≥ 1 and adjusted p-value < 0.05, with multiple testing correction via the Benjamini–Hochberg method. For enhanced stringency, DESeq2 results were integrated with intensity difference filtering in SeqMonk.

Heatmaps and principal component analysis (PCA) plots were produced in SeqMonk. Gene ontology (GO) analysis was performed on significantly upregulated and downregulated genes, with enriched GO terms identified using DAVID [31], applying a Benjamini-adjusted p-value threshold of < 0.05.

Raw label-free quantitative proteomics data were analyzed in R (version 4.5.1) using the *Differential Enrichment analysis of Proteomics data* (DEP) package (version 1.26.0). Protein intensity values were imported from a pre-processed matrix containing LFQ (label-free quantification) intensities, previously generated using the DIA-NN protein quantification software.

Proteins with missing values in any sample were excluded by applying a strict missing-value threshold of zero, retaining only those quantified across all samples. The resulting dataset was normalized using variance stabilizing normalization (VSN) to minimize technical variation between samples. Differential enrichment analysis was then performed, with the control group explicitly defined. Proteins were considered significantly regulated if they exhibited an absolute fold change > 1.5 and an adjusted p-value < 0.05. Significant proteins were extracted based on these criteria.

BAP1-OE gene signature interrogation was performed as described in [32], including unsupervised clustering and principal component analysis (PCA) to evaluate the ability of the gene list to separate the groups within each dataset. Hierarchical clustering heatmaps were generated using the gplots R package with Euclidean distance. Individual PCA plots were generated with the factoextra R package.

Single-sample Gene Set Enrichment Analysis (ssGSEA) was performed using the GSVA R package to compute enrichment scores (ES) for the BAP1-OE gene signature in individual samples. The signature was evaluated across placental transcriptomic datasets of early-onset pre-eclampsia (EO-PE; GSE114691 and GSE190971) and additional pregnancy complications associated with placental dysfunction, including intrauterine growth restriction (IUGR; GSE220877), gestational diabetes mellitus (GDM; GSE203346), and COVID-19 infection (GSE171995). Differences in ssGSEA ES between case and control groups were assessed using an unpaired two-tailed Student's t test. The diagnostic performance of the BAP1-OE signature in discriminating EO-PE from controls was evaluated using the pROC R package. ROC curves were generated from ssGSEA ES values, and the area under the curve (AUC), sensitivity, specificity, and optimal threshold (Youden index) were calculated.

For data exploration and visualization, PCA, volcano plots, hierarchical clustering heatmaps, and sample correlation plots were generated using a combination of DEP-native and custom R functions. Functional enrichment analysis of significantly regulated proteins was performed using Gene Ontology (GO) terms, and resulting p-values were transformed to $-\log_{10}$ for graphical representation in bar plots. Protein–protein interaction networks were constructed using the STRING database (version 11).

Quantification and statistical analysis

All statistical procedures, including sample sizes (n), number of independent experiments, and specific tests applied, are detailed in the "Methods Section" and in each figure legend. In brief, human placental sample comparisons (Fig. 1) were performed using Student's two-tailed t-tests or one-way ANOVA, depending on the number of groups. Data from human samples are presented as median ± interquartile range, and sample sizes were limited by the availability of rigorously phenotyped placental material (Supplementary File 1). For cell-line experiments, each dataset represents ≥3 independent experiments. Unless otherwise specified, quantitative data from cell-line–based assays are presented as mean ± SEM. Proliferation analyses (Fig. 2D Supplementary Fig. 2E) were performed using two-way ANOVA with Holm–Sidak post hoc correction. Adhesion assays (Fig. 2E; Supplementary Fig. 2F), western blot quantification (Figs. 1C and 2B, C; 5D; Supplementary Fig. 2C), and organoid area measurements (Supplementary Fig. 5B, F) were analysed using Student's two-tailed t-tests, where n refers to the number of independent experiments or individual organoids, as specified in the figure legends. RT-qPCR and western blot analyses of PR-DUB complex dynamics during trophoblast differentiation were performed using one-way ANOVA with Dunnett's multiple-comparisons test (Fig. 1A, B). RT-qPCR datasets quantifying lineage marker expression during EVT and STB differentiation (Figs. 3C, 4C and Supplementary Figs. 3A, 4A, B), HLA-G and SDC1 western blot quantification (Figs. 3B, 4B), and zymography (Supplementary Fig. 3B) were analysed using two-way ANOVA with Tukey's multiple-comparisons test, with n representing the number of independent experiments.

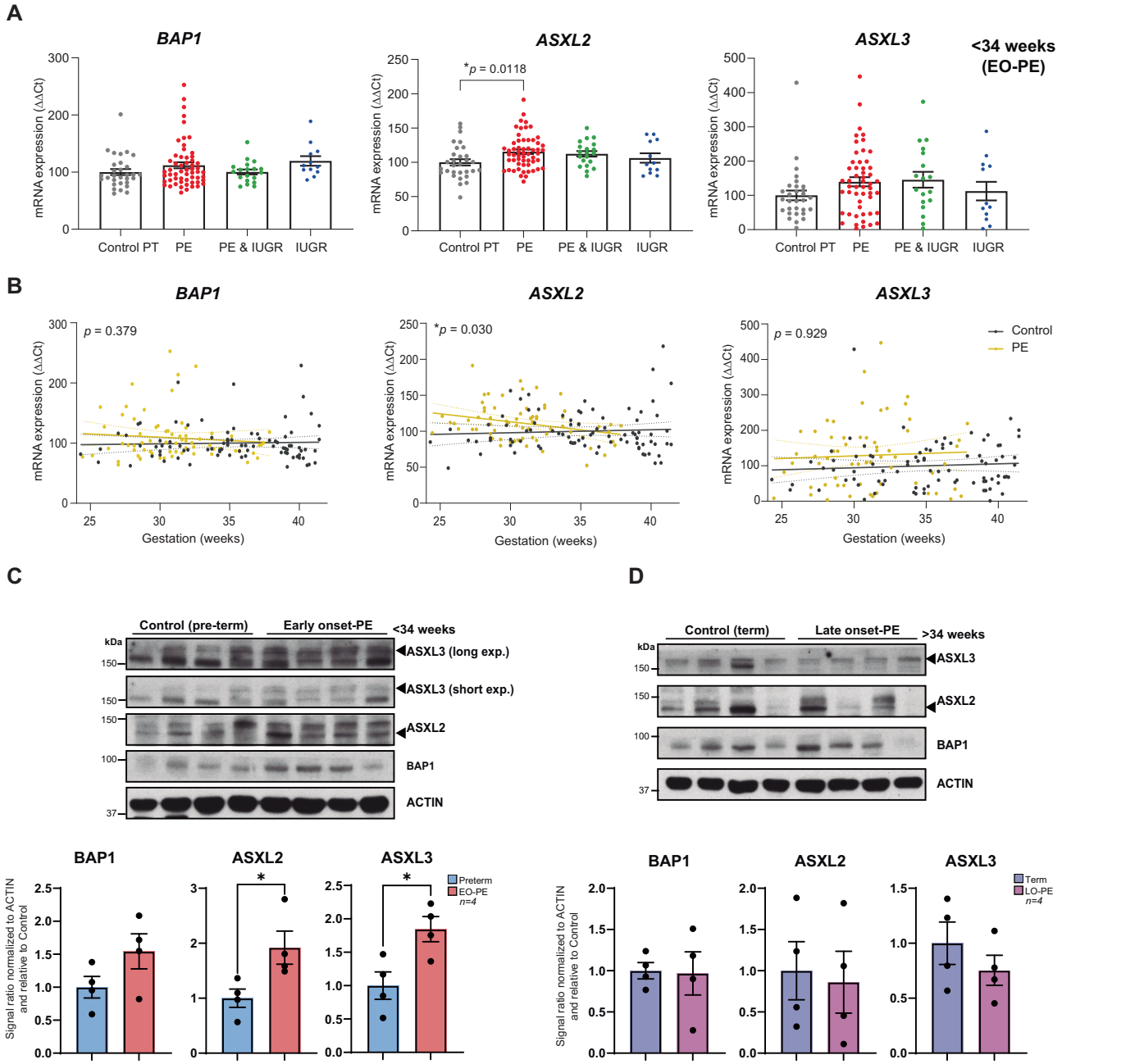

Fig. 1 BAP1 PR-DUB complex levels in placental tissue from pregnancies with complications. A Relative mRNA expression of *BAP1*, *ASXL2*, and *ASXL3* in central villous placental biopsies collected before 34 weeks of gestation from gestational age–matched control pregnancies (Control PT; preterm, $n = 30$), preeclampsia (PE, $n = 56$), PE with intrauterine growth restriction (PE&IUGR, $n = 19$), or IUGR alone ($n = 12$). Data are presented as median ± interquartile range. Statistical analysis was performed using one-way ANOVA with Kruskal–Wallis multiple comparisons test. **B** mRNA levels of *BAP1*, *ASXL2*, and *ASXL3* were increased in early-onset PE (EO-PE), with *ASXL2* showing a significant association with gestational age at delivery ($p = 0.030$). Associations were assessed using simple linear regression. $p < 0.05$. **C** Western blot analysis of BAP1, ASXL2, and ASXL3 protein levels in Control PT and EO-PE placentas (< 34 weeks) from an independent cohort confirmed increased protein levels of the BAP1 PR-DUB complex in EO-PE. Graphs show quantification from four independent biological replicates. Data are presented as mean ± SEM; $p < 0.05$ (Student's *t* test). **D** Western blot analysis of BAP1, ASXL2, and ASXL3 protein levels in late-onset PE (LO-PE) revealed no significant differences compared to Control PT. Graphs show quantification from four independent biological replicates. Data are presented as mean ± SEM (Student's *t* test).

RNA-seq differential expression analysis was performed using DESeq2, with significance defined as adjusted $p < 0.05$ (Benjamini–Hochberg correction) and $|\log_2 FC| \geq 1$. PCA, volcano plots, hierarchical clustering, and GO analyses were generated using SeqMonk or R, as described (Figs. 2F, 3D, 4D, E, 5E and Supplementary Figs. 2J, 3C–E, 4C–H, 5G; Supplementary Files 3–4). Proteomics data were re-processed using DIA-NN for peptide quantification and the DEP R package for differential protein analysis. To minimize false positives, a stringent threshold of adjusted $p < 0.05$ and FC > 1.5 was applied across all proteomic datasets (Figs. 2G, H, 3E, F, 4F and Supplementary Figs. 4I, 5H–I; Supplementary Files 5–6). To define the BAP1-OE gene signature, only transcripts and proteins showing concordant differential regulation in both RNA-seq and proteomics were retained (Fig. 5F and Supplementary File

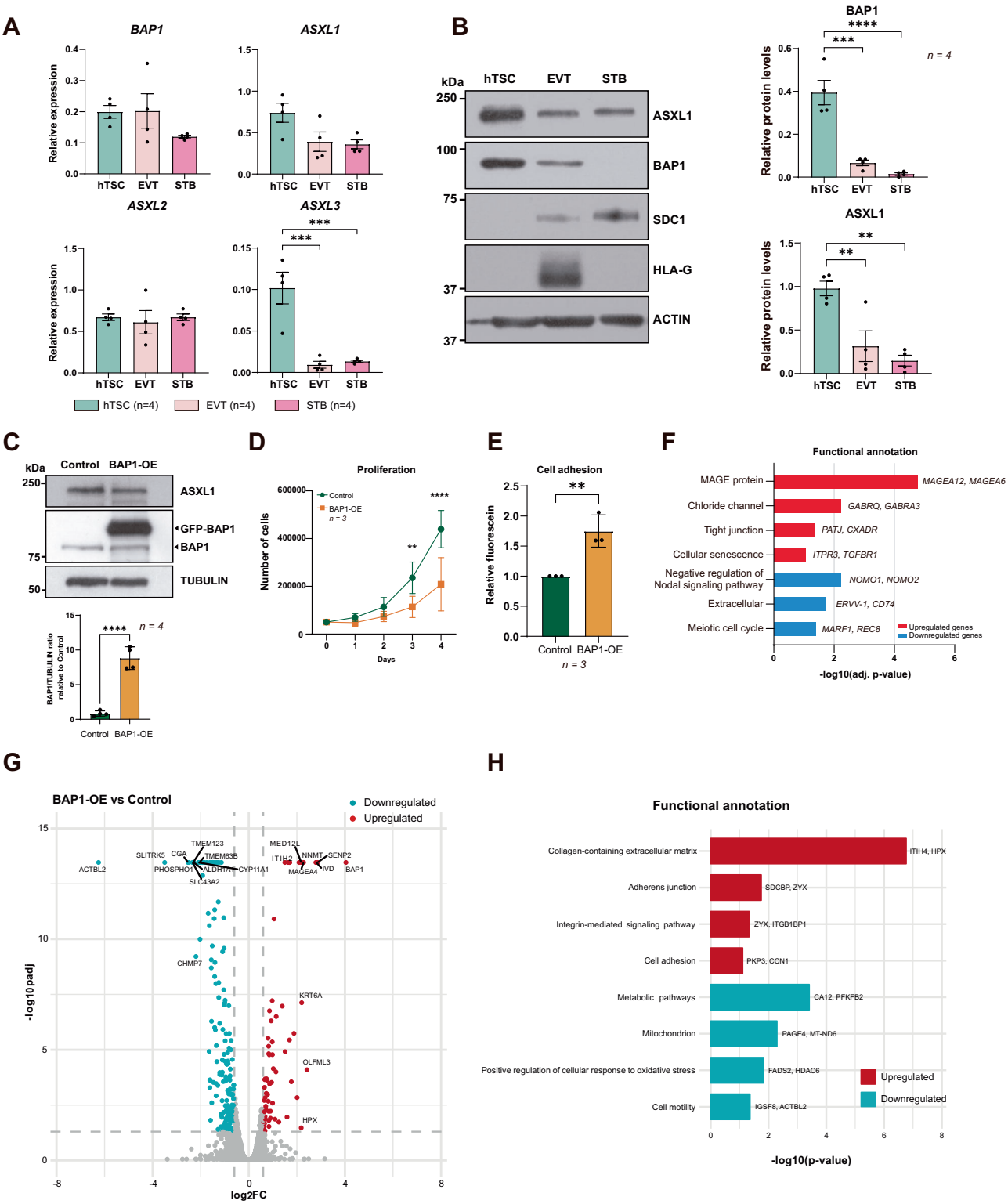

7). Enrichment of this signature in placental datasets was quantified using ssGSEA. ROC analyses were performed using the pROC R package to evaluate diagnostic performance in EO-PE versus controls (Fig. 5G and Supplementary Fig. 5J–K), with AUC, sensitivity, specificity, and optimal thresholds computed using the Youden index. All statistical analyses were performed using GraphPad Prism v9.4.1 and R (v2024.09.1). Statistical significance was defined as $p < 0.05$.

RESULTS

BAP1 and PR-DUB components are upregulated in early-onset preeclampsia placentas

To explore whether BAP1 dysregulation is associated with preeclampsia, we analyzed placental tissues from two independent cohorts of pregnancies complicated by early-onset PE (EO-PE) and intrauterine growth restriction (IUGR). RT-qPCR analysis

Fig. 2 BAP1 downregulation is essential for early placental development. A mRNA expression levels of PR-DUB components (*BAP1, ASXL1, ASXL2*, and *ASXL3*) in human trophoblast stem cells (hTSCs), extravillous trophoblasts (EVT), and syncytiotrophoblasts (STBs), quantified by RT-qPCR. Data represent mean ± SEM of $n = 4$ independent experiments; ***$p < 0.001$; one-way ANOVA with Dunnett's multiple comparisons test. **B** Western blot analysis of PR-DUB subunits (ASXL1 and BAP1) and lineage markers (SDC1 as a STB marker, HLA-G as an EVT marker) with ACTIN as a loading control, across differentiation states. ACTIN or TUBULIN was used as a loading control, as indicated, and each target protein was normalized to the corresponding loading control within the same experiment. Quantification of BAP1 and ASXL1 protein levels relative to the loading control is shown on the right, confirming ASXL1 and BAP1 downregulation during differentiation. Data are mean ± SEM of $n = 4$ independent experiments; **$p < 0.005$, ***$p < 0.001$, ****$p < 0.0001$; one-way ANOVA with Dunnett's multiple comparisons test. **C** Western blot of ASXL1, endogenous BAP1, GFP-tagged BAP1 (GFP-BAP1), and TUBULIN (loading control) in BAP1-OE and Control hTSCs. Quantification of BAP1/TUBULIN ratio is plotted on the bottom (mean ± SEM, $n = 4$ independent experiments; ****$p < 0.0001$; Student's two-tailed t-test). **D** Proliferation rates of BAP1-OE and control hTSCs over 4 days, showing significantly reduced cell numbers at days 3 and 4 (mean ± SEM, $n = 3$ independent experiments; two-way ANOVA with Holm-Sidak's post hoc test) **E** Adhesion assay quantifying fluorescein-labeled BAP1-OE hTSCs relative to controls (mean ± SEM, $n = 3$ independent experiments; **$p < 0.005$; Student's two-tailed t-test). **F** Functional enrichment analysis of DEGs, highlighting pathways associated with upregulated (red) and downregulated (blue) genes. **G** Volcano plot of differentially expressed proteins (DEPs) in BAP1-OE hTSCs compared to control hTSCs (red: upregulated proteins; blue: downregulated proteins; adjusted $p < 0.05$, FC > 1.5). **H** Functional enrichment analysis of DEPs, highlighting pathways associated with upregulated (red) and downregulated (blue) proteins. OE overexpression.

revealed an overall trend toward upregulation of *BAP1*, *ASXL2*, and *ASXL3* mRNA in EO-PE samples, with the increase in *ASXL2* reaching statistical significance, whereas *ASXL1* levels remained unaltered (Fig. 1A and Supplementary Fig. 1A). This expression profile was predominantly observed before 34 weeks of gestation (Fig.1B and Supplementary Fig 1B). Western blot analysis of an independent cohort corroborated these findings at the protein level: placentas from EO-PE cases exhibited elevated BAP1, ASXL2, and ASXL3 expression compared to gestationally matched control (control pre-term), whereas late-onset PE (LO-PE) samples showed no significant changes compared to gestationally matched control samples at term (Fig. 1C, D quantifications below). These data indicate that BAP1-PR-DUB complex dysregulation is specifically associated with EO-PE.

BAP1 regulates epithelial identity in human trophoblast stem cells

Previously, we have demonstrated that BAP1 is highly expressed in proliferative CTB within first-trimester human placentas but is markedly reduced in differentiated EVT and even further diminished in STB [24]. Given its dynamic expression during in vivo differentiation, we here examined the role of the BAP1 PR-DUB complex in undifferentiated hTSCs and across hTSCs in vitro differentiation. RT-qPCR analysis showed that *ASXL1* was highly expressed in hTSCs under stem cell conditions and became markedly downregulated during trophoblast differentiation, both in EVT and STB. *ASXL3* mRNA levels also decreased upon differentiation, whereas BAP1 expression remained relatively stable, and *ASXL2* displayed only minor changes across differentiation. The expression patterns observed in EVT were consistent with our previous findings [24], and here we extend these analyses to STB differentiation (Fig. 2A). At the protein level, ASXL1 was highly expressed under self-renewing conditions, while both BAP1 and ASXL1 levels declined upon EVT or STB differentiation (Fig. 2B). Knockdown of BAP1 via CRISPR/Cas9-mediated deletion of exon 4 in bulk BTS11 hTSCs led to increased proliferation and reduced cell adhesion, without compromising the stem cell marker profile (Supplementary Fig. 2A–G). Conversely, BAP1 overexpression (BAP1-OE) resulted in decreased proliferation and enhanced adhesion, with no gross morphological alterations (Fig. 2C–E and Supplementary Fig. 2H, I). To explore the molecular consequences of BAP1 overexpression, we performed RNA-seq analysis on both control and BAP1-OE hTSCs. This analysis identified 54 differentially expressed genes (DEGs) regulated by BAP1 overexpression (28 genes upregulated and 26 genes downregulated, p-value < 0.05; $\log_2$FC > 1) (Supplementary Fig. 2J and Supplementary file 3). In line with our previous observations of increased epithelial markers in BAP1-OE hTSCs, Gene Ontology (GO) analysis of BAP1-OE hTSCs revealed enrichment of gene programs related to cell adhesion, tight junction assembly, and epithelial integrity, alongside downregulation of cell cycle and metabolic regulators (Fig. 2F and Supplementary file 4).

Proteomic profiling (Differentially Expressed Proteins; DEP, FC > 1.5, p-adjusted < 0.05) further confirmed that BAP1-OE cells exhibit increased abundance of proteins involved in the regulation of the collagen-containing extracellular matrix, adherens junction, integrin-mediated signaling pathways, and cell adhesion—hallmarks of reinforced epithelial traits—while downregulated proteins were enriched for functions related to metabolic pathways, mitochondrion, positive regulation of cellular response to oxidative stress and cell motility (Fig. 2G, H and Supplementary files 3 and 4). These findings indicate that BAP1 promotes an epithelial-like, adherent trophoblast state that is antagonistic to differentiation.

Forced BAP1 expression delays EVT differentiation and invasion capacity

To assess the impact of BAP1 on EVT generation, we differentiated control and BAP1-OE and BAP1-KD hTSCs for 8 days. Control and BAP1-KD cells successfully differentiated into EVTs, acquiring spindle-like mesenchymal morphology and upregulated canonical EVT markers, including *HLA-G*, *MMP2*, *ITGA5*, and *PLAC8*, with no significant differences between BAP1-KD and controls (Supplementary Fig. 3A). In contrast, BAP1-OE cells formed compact aggregates with attenuated HLA-G expression (Fig. 3A, B). RT-qPCR analyses demonstrated impaired induction of EVT markers, including *HLA-G*, *ITGA5*, *FSTL3*, *NOTUM*, and *MMP2* in BAP1-OE cells compared to control hTSCs (Fig. 3C). Zymography confirmed reduced MMP2 enzymatic activity (Supplementary Fig. 3B). Transcriptomic profiling (DESeq2, $\log_2$FC > 1, p-value < 0.05) revealed that BAP1-OE EVTs retained expression of progenitor and early-EVT markers while failing to activate genes associated with mature EVT identity and extracellular matrix remodeling [33] (Fig. 3D and Supplementary Fig. 3C, D; Supplementary files 3 and 4). Differential proteomic analysis (FC > 1.5, p-adjusted < 0.05) identified 60 proteins significantly upregulated and 37 downregulated in BAP1-OE EVTs compared to control cells (Fig. 3E and Supplementary file 5). Gene Ontology analysis showed that upregulated proteins were primarily enriched in pathways related to focal adhesion, actin binding, cell junction organization, and cell adhesion. In contrast, the downregulated proteins were enriched in categories related to female pregnancy, L-glutamine transmembrane transporter activity and peptidase M10 metallopeptidase activity (Fig. 3F and Supplementary Fig. 3D; Supplementary file 6). Together, these results demonstrate that BAP1 overexpression perturbs EVT differentiation and impairs ECM remodeling.

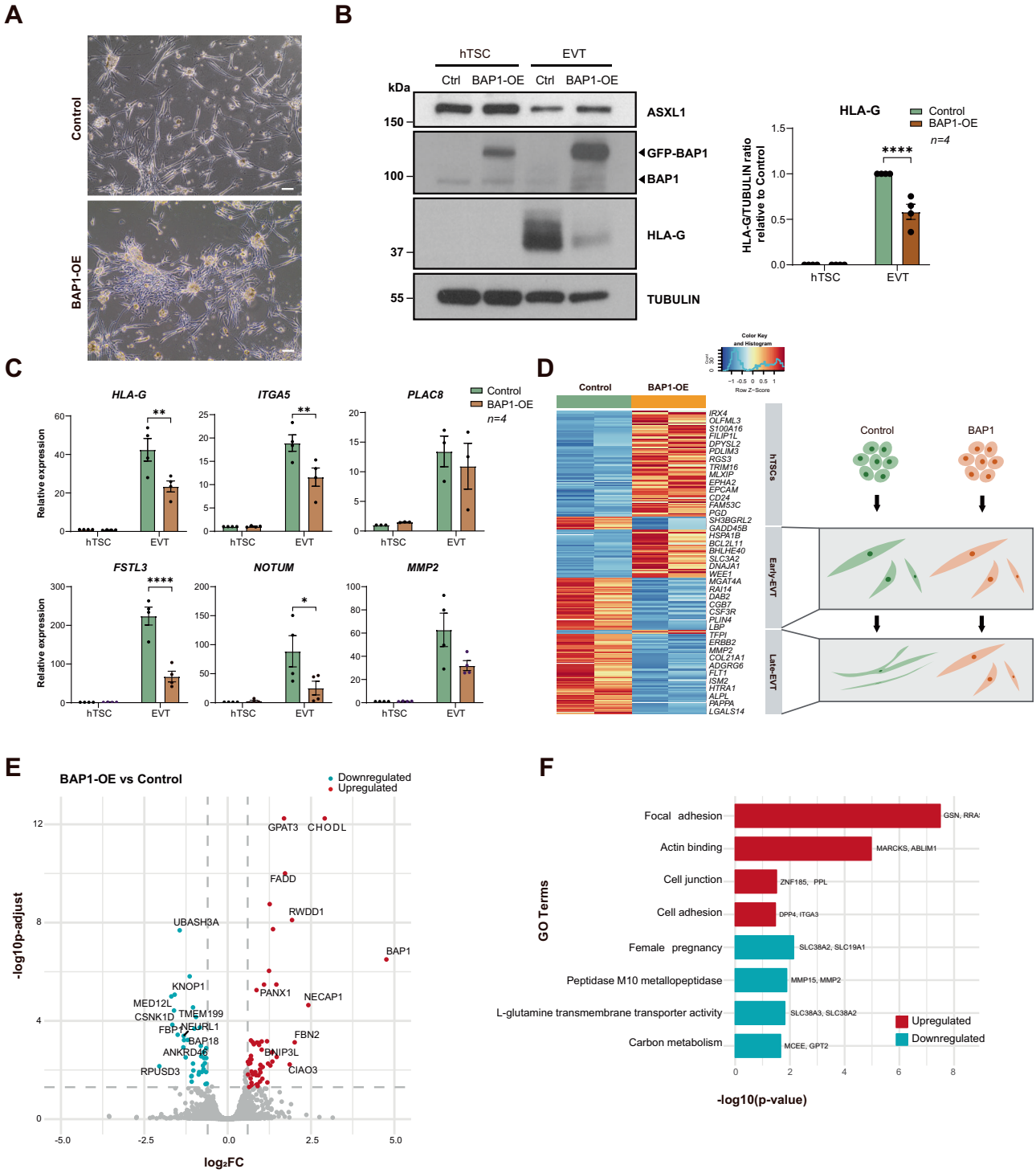

Fig. 3 BAP1 overexpression impairs extravillous trophoblast formation and function. A Phase contrast images of EVTs showing aggregated colony morphology with reduced elongation in BAP1-OE cells versus control EVTs. Scale bars, 150 µm. **B** Western blot analysis of ASXL1, BAP1, GFP-BAP1, HLA-G and TUBULIN (loading control) in BAP1-OE hTSC and EVTs compared to control cells. Quantification of HLA-G/TUBULIN ratio relative to control cells growing in stem cell conditions is plotted on the right (mean ± SEM, $n = 4$ independent experiments; ****$p < 0.0001$; two-way ANOVA with Tukey's multiple comparisons test. **C** RT-qPCR analysis of EVT-specific (*HLA-G, ITGA5, PLAC8, FSTL3, NOTUM, MMP2*) markers in BAP1-OE hTSC and EVTs compared to control cells (mean ± SEM, $n = 4$ independent experiments; *$p < 0.05$, **$p < 0.01$, ****$p < 0.0001$; two-way ANOVA with Tukey's multiple comparisons test. **D** On the left, heatmap of stage-specific marker expression (row-scaled Z-scores) in BAP1-OE EVTs versus control EVTs, showing retention of early-EVT markers (*DAB2*, *LBP*) and failure to activate late-EVT (*MMP2*, *FLT1*) transcriptional programs. Gene clusters defined by Kim et al., 2024. On the right, schematic model of differentiation blockade, demonstrating how BAP1 overexpression prevents progression from early to late EVT states. **E** Volcano plot of differentially expressed proteins (DEPs) in BAP1-overexpressing EVTs compared control EVTS (red: upregulated proteins; blue: downregulated proteins; adjusted $p < 0.05$, FC > 1.5). **F** Gene ontology enrichment analysis of DEPs, highlighting pathways associated with upregulated (red) and downregulated (blue) proteins. EVT extravillous trophoblast, hTSC human trophoblast stem cell, OE overexpression.

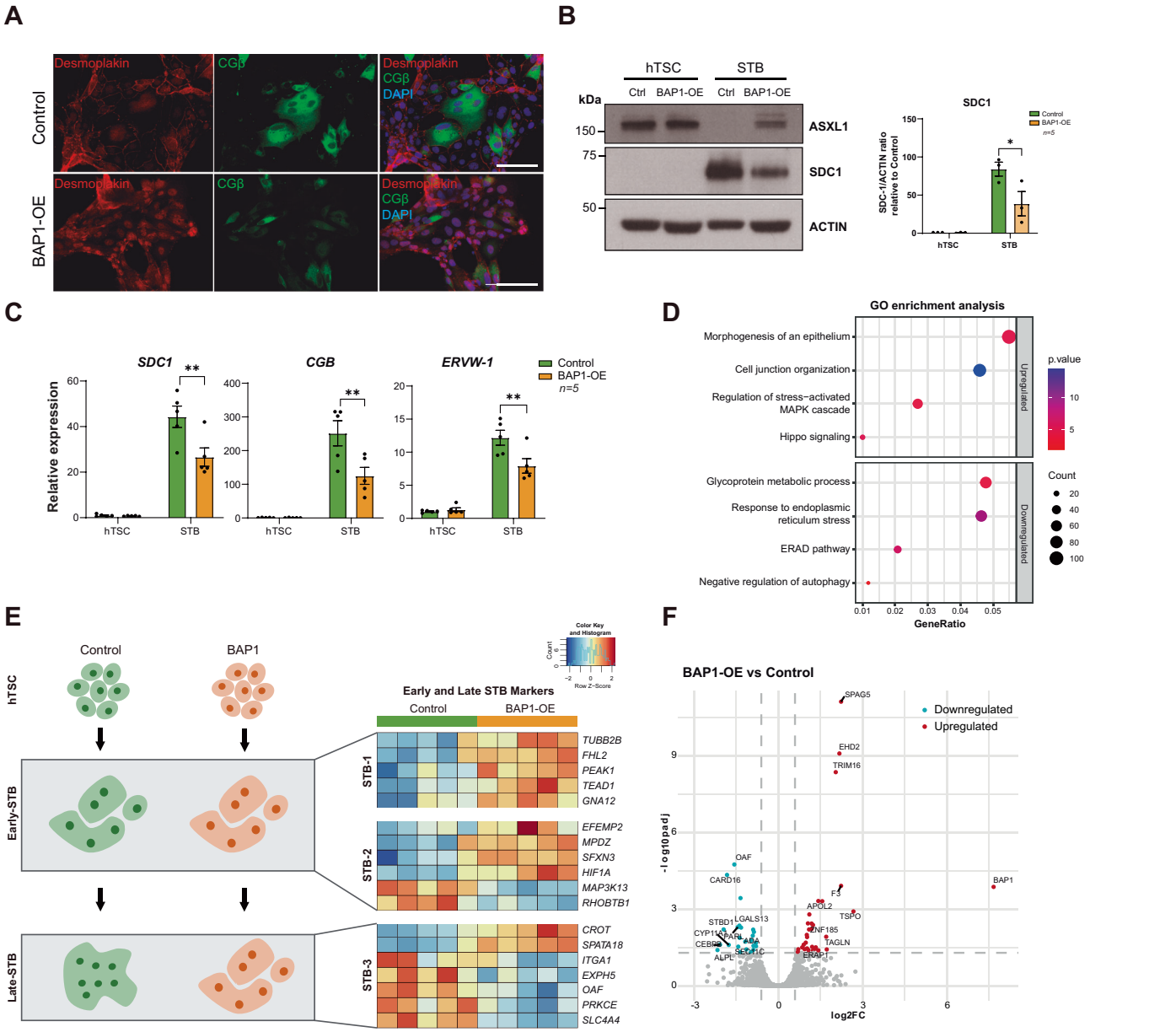

Fig. 4 BAP1 overexpression impairs syncytiotrophoblast formation and function. A Immunofluorescence of Desmoplakin and CGβ in BAP1-OE and Control STBs, with DAPI nuclear counterstain. Scale bars, 150 µm. **B** Western blot of ASXL1, SDC1 and ACTIN (loading control) expression in BAP1-OE hTSC and STBs compared to control cells. Quantification of SDC1/ACTIN ratio relative to control hTSCs is plotted on the right (mean ± SEM, $n = 4$ independent experiments; *$p < 0.05$, two-way ANOVA with Tukey's multiple comparisons test). **C** RT-qPCR analysis of STB-specific (*SDC1*, *CGB*, *ERVW-1*) markers in BAP1-OE hTSC and STBs compared to control cells (mean ± SEM of $n = 4$ independent experiments; **$p < 0.005$, two-way ANOVA with Tukey's multiple comparisons test). **D** GO analysis of differentially expressed genes in BAP1-OE versus control STBs, highlighting upregulated and downregulated pathways. **E** On the left, a schematic of impaired cell fusion in BAP1-overexpressing cells, leading to defective STB formation. On the right, a heatmap of FPKM values for STB lineage markers (STB-1, STB-2, and STB-3), representing progressive differentiation states, from early to late STB states, in BAP1-OE and Control STBs. Data are z-score normalized across rows. **F** Volcano plot of differentially expressed proteins (DEPs) in BAP1-overexpressing STBs versus Controls (red: upregulated proteins; blue: downregulated proteins; adjusted $p < 0.05$, FC > 1.5). hTSC human trophoblast stem cell, OE overexpression, STB syncytiotrophoblast.

BAP1 overexpression impairs syncytiotrophoblast differentiation and function

To determine whether BAP1 also impairs STB formation, we induced syncytialization in BAP1-OE, BAP1-KD and control hTSCs under 2D conditions. Control and BAP1-KD cells displayed typical multinucleation and upregulated syncytial markers, including *SDC1*, *CGB*, *ERVW-1* and *ERVFRD-1* with no significant differences between BAP1-KD and controls, indicating that BAP1 downregulation does not impair STB differentiation (Supplementary Fig. 4A). In contrast, BAP1-OE cells retained epithelial morphology, exhibited diminished fusion, and showed impaired upregulation of STB genes (Fig. 4A–C and Supplementary Fig. 4B)). Notably, *ASXL1* and *ASXL3* transcript levels remained elevated in BAP1-OE cells, consistent with a stalled differentiation state (Supplementary Fig. 4B).

Transcriptomic analysis (DESeq2; log2FC > 1, *p-value* < 0.05) indicated downregulation of ER stress response, autophagy, pregnancy hormone regulation, and glycoprotein metabolism pathways, features typically enhanced during syncytialization, while epithelial junction, hippo signaling, focal adhesion, stem cell proliferation, and

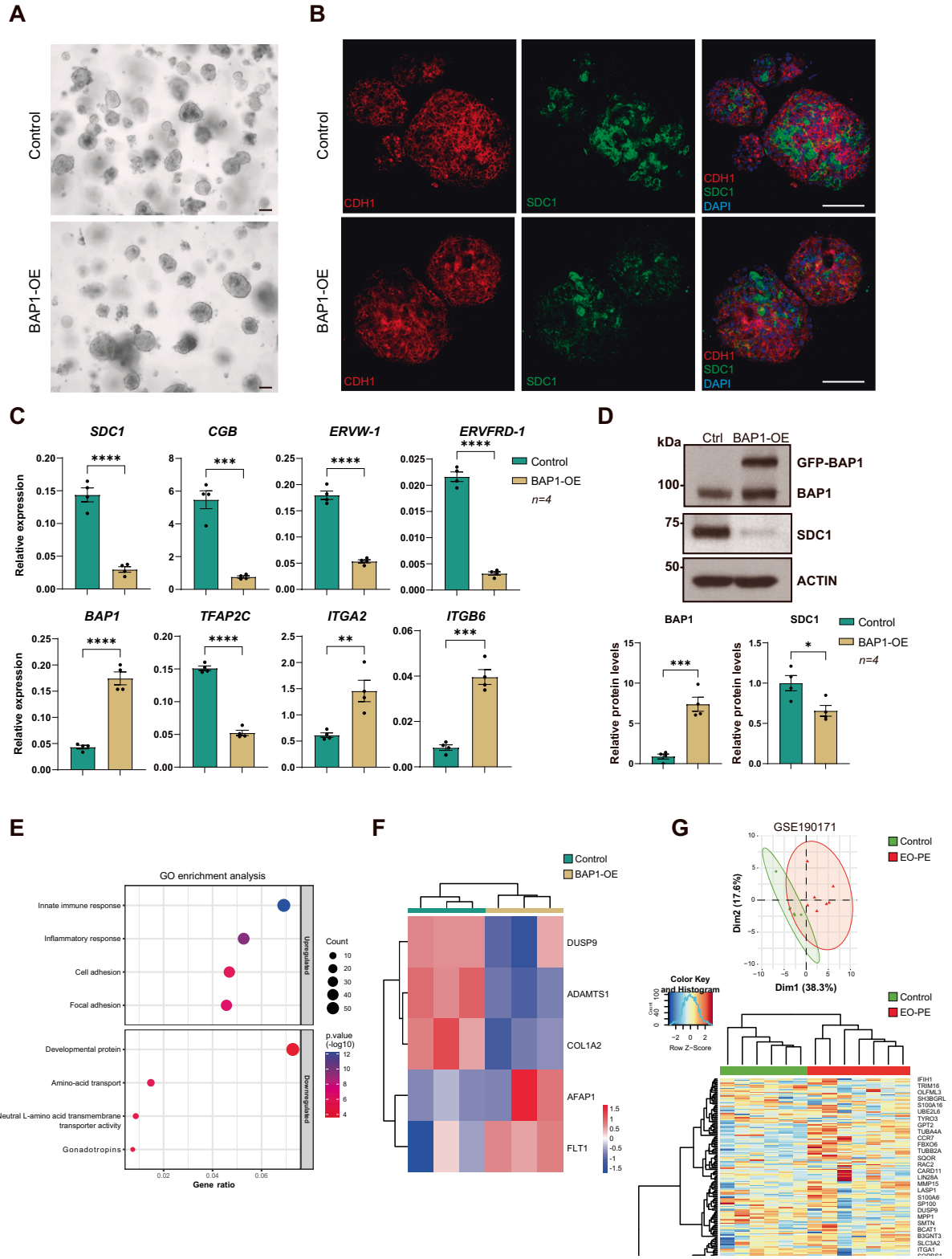

programs were upregulated (Fig. 4D and Supplementary Fig. 4C–H). Consistently, comparison of DEGs to known early- and late-STB markers [34] showed that control STBs upregulated late-STB markers (*ITGA1, EXPH5, OAG, PRKCE*, and *SLC4A4*), whereas BAP1-OE cells remained in an early-STB state, characterized by expression of early-STB markers such as *TUBB2B, FHL2, PEAK1, TEAD1, GNA12, EFEMP2, MPDZ, SFXN3*, and *HIF1A* (Fig. 4E).

Comprehensive proteomic profiling revealed that BAP1-OE STBs displayed 31 significantly upregulated and 24 downregulated proteins compared to controls (FC > 1.5, adjusted $p < 0.05$; Fig. 4F and Supplementary file 5). GO analysis showed that upregulated proteins were enriched in pathways related to focal adhesion, actin binding, cell adhesion and cell-matrix organization, consistent with reinforcement of epithelial traits. In contrast,

Fig. 5 BAP1 overexpression disrupts trophoblast organoid formation and recapitulates early-onset preeclampsia features. A Brightfield images of BAP1-OE and control organoids, demonstrating comparable morphology and size. Scale bar, 150 µm. **B** Immunofluorescence (IF) staining of BAP1-OE and control organoids for CDH1 and SDC1. Nuclear counterstaining was with DAPI. Scale bars, 150 µm. **C** RT-qPCR analysis of STB (*SDC1*, *CGB*, *ERVW-1*, and *ERVFRD-1*), *BAP1*, stem cell (*TFAP2C)* and villous cytotrophoblast cell column (*ITGA2*, *ITGB6*) markers in BAP1-OE and control organoids (mean ± SEM, $n = 4$ independent experiments; $^{**}p < 0.005$, $^{***}p < 0.001$, $^{****}p < 0.0001$; Student two-tailed t-test). **D** Western blot analysis of BAP1, GFP-BAP1, and SDC1 in BAP1-OE and control organoids, with ACTIN or HSP90 used as loading controls, as indicated. Each target protein was normalized to its corresponding loading control within the same experiment. Quantification of relative BAP1 and SDC1 protein levels, expressed relative to control organoids, is shown at the bottom (mean ± SEM, $n = 3$ independent experiments; $p < 0.05$, $^{**}p < 0.001$; Student's two-tailed *t*-test). **E** GO enrichment analysis of differentially expressed genes (DEGs) in BAP1-OE *vs* control organoids. **F** Heatmap showing representative proteins from the BAP1-OE signature that are also dysregulated in PE, with downregulation of DUSP9, ADAMTS1, and COL1A2, and upregulation of AFAP1 and FLT1 in BAP1-OE organoids. Colour scale indicates scaled expression values (red, upregulation; blue, downregulation). **G** (Upper panel) Principal component analysis (PCA) plots showing the distribution of early-onset preeclampsia (EO-PE) samples (red) and controls (green) from the GSE190171 EO-PE-affected dataset, based on the BAP1-OE molecular signature. The X and Y axes represent principal components 1 and 2, which explain the indicated percentage of total variance. (Lower panel) Unsupervised hierarchical clustering of EO-PE (red) and control (green) samples from each dataset, based on the BAP1 gene signature. OE, overexpression; STB, syncytiotrophoblast.

downregulated proteins were associated with mitochondrial inner membrane, protein folding in the endoplasmic reticulum, and metabolic pathway function (Supplementary Fig. 4I and Supplementary File 6). Collectively, these results demonstrate that BAP1 overexpression obstructs STB fate acquisition.

BAP1-OE trophoblast organoids mirror preeclampsia features

Trophoblast organoids, which closely resemble first-trimester placental villi, provide a physiologically relevant model for studying human placental development [6, 7]. These 3D structures consist of an outer layer of proliferative CTBs that spontaneously differentiate into STBs within the organoid core. To validate our findings, we cultured BAP1-OE, BAP1-KD, and control hTSCs as trophoblast organoids. Consistent with findings in 2D cultures, BAP1-KD organoids exhibited a larger size than controls, indicative of enhanced proliferation (Supplementary Fig. 5A, B). BAP1-KD organoids displayed defects in STB differentiation, including reduced SDC1 staining, disorganized CDH1 localization in the CTB layer, and downregulation of canonical STB markers (*SDC1*, *CGB*) (Supplementary Fig. 5C, D), suggesting compromised epithelial integrity and altered STB differentiation timing. BAP1-OE organoids also exhibited markedly reduced central syncytial regions (Fig. 5A, B and Supplementary Fig. 5E, F). Immunofluorescence and RT-qPCR analyses revealed downregulation of STB markers, including *SDC1*, *CGB*, *ERVW1*, and *ERVFRD-1*, alongside increased expression of CTB-associated integrins *ITGA2* and *ITGB6* (Fig. 5B, C and Supplementary Fig. 5E, F). Western blot analysis further confirmed impaired STB differentiation, as BAP1-OE organoids failed to upregulate SDC1, a key mediator of syncytial maturation (Fig. 5D).

RNA-seq revealed a profound impact of BAP1 overexpression on the organoid transcriptome, identifying 1936 differentially expressed genes (DESeq2; $\log_2FC > 1$, $p < 0.05$), with 972 upregulated and 964 downregulated transcripts (Supplementary File 3). Principal component analysis (PCA) showed clear segregation of samples based on intracellular BAP1 levels (Supplementary Fig. 5G and Supplementary File 3). Gene ontology (GO) enrichment analysis indicated that upregulated genes were enriched for innate immune and inflammatory responses, focal adhesion, and cell adhesion pathways. In contrast, downregulated genes were associated with developmental protein, amino acid transport, neutral L-amino acid transmembrane transporter activity, and gonadotropin expression, features typically linked to impaired STB maturation (Fig. 5E and Supplementary File 4).

Complementary proteomic profiling identified 102 significantly upregulated and 63 downregulated proteins in BAP1-OE organoids (FC > 1.5, adjusted $p < 0.05$; Supplementary File 3). Reactome Pathway and GO analysis using STRING revealed enrichment of interferon signaling, cytokine signaling, MHC class I peptide folding and loading, ER-phagosome, and endosomal and vacuolar trafficking (Supplementary Fig. 5H). Proteins related to extracellular matrix organization, extracellular region and space, and endoplasmic reticulum lumen were significantly downregulated, reinforcing a disruption in STB differentiation (Supplementary Fig. 5I).

Integrated transcriptomic and proteomic analyses demonstrate that BAP1 overexpression induces a pro-inflammatory, progenitor-like state that is incompatible with proper syncytiotrophoblast maturation, a phenotype that mirrors key pathological features of EO-PE, including heightened interferon signaling and dysregulated immune–trophoblast interactions [35]. To further investigate this association, we defined a BAP1-OE gene signature by integrating transcriptomic and proteomic data across STB, EVT, and trophoblast organoid models. Differentially expressed genes (DEGs; DESeq2, $\log_2FC > 1$, adjusted $p < 0.05$) and differentially expressed proteins (DEPs; FC > 1.5, $p < 0.05$) between control and BAP1-OE conditions showing concordant directional changes were retained (Supplementary File 7), providing a robust representation of BAP1-driven trophoblast states. When applied to trophoblast organoids, the BAP1-OE signature revealed dysregulation of genes previously linked to PE, including downregulation of DUSP9, ADAMTS1, and COL1A2, and upregulation of AFAP1 and FLT1 (Fig. 5F) [36–40]. The BAP1-OE gene signature was next interrogated across two independent EO-PE placental datasets (GSE114691 and GSE190971), as well as datasets representing other pregnancy complications associated with placental dysfunction, including intrauterine growth restriction (IUGR; GSE220877), gestational diabetes mellitus (GDM; GSE203346), and COVID-19 (GSE171995). In EO-PE cohorts, the BAP1 signature achieved an average sensitivity of 48.5%, specificity of 97.5%, and a mean AUC of 0.71, indicating strong discriminatory power with minimal false-positive classification. In contrast, the signature showed limited or no discriminatory capacity in IUGR, GDM, or COVID-19 placentas, underscoring its specificity for EO-PE–related placental alterations (Supplementary File 7). Principal component analysis (PCA) and unsupervised hierarchical clustering further confirmed a clear segregation of EO-PE from control samples, whereas other pregnancy disorders displayed overlapping transcriptional profiles (Fig. 5G; Supplementary Fig. 5J, K). Together, these findings indicate that the BAP1-driven molecular program constitutes a distinct feature of EO-PE placentas and provide a mechanistic link between BAP1 dysregulation, impaired STB lineage commitment, and the pathogenesis of early-onset preeclampsia.

DISCUSSION

This study identifies BAP1 as a central regulator of human trophoblast differentiation, with direct implications for placental development and the pathogenesis of early-onset preeclampsia (EO-PE). By integrating transcriptomic, proteomic, and functional

data across 2D and 3D models, we demonstrate that BAP1 must be downregulated to enable lineage commitment toward both extravillous trophoblast (EVT) and syncytiotrophoblast (STB) fates. In contrast, sustained BAP1 expression maintains a progenitor-like, epithelial state and impairs terminal differentiation, providing a mechanistic link to the trophoblast dysfunction characteristic of EO-PE placentas.

Previous studies in mice have shown that *Bap1* deletion causes mid-gestation lethality due to placental defects, including impaired chorionic ectoderm differentiation and failure of labyrinth formation, which compromises maternal–fetal exchange [20, 41]. These defects have been linked to abnormal syncytiotrophoblast development and an excess of trophoblast giant cells, indicating a role for BAP1 in trophoblast lineage specification. At the molecular level, downregulation of BAP1 in mouse trophoblast stem cells promotes trophoblast epithelial–mesenchymal transition (EMT) characterized by reduced epithelial features, acquisition of mesenchymal and invasive traits, and enhanced trophoblast invasiveness [24]. However, whether this function is conserved in humans and whether it contributes to pregnancy complications has remained unclear.

Here, we show that BAP1 is highly expressed in human trophoblast stem cells (hTSCs) and undergoes robust downregulation during differentiation toward both EVT and STB lineages. Gain- and loss-of-function experiments reveal that persistent BAP1 expression stabilizes epithelial identity, enhances cell adhesion, and represses transcriptional programs required for lineage progression. These findings are consistent with BAP1's role in maintaining epithelial organization in other tissues, such as the liver [42], and underscore the broader role of BAP1 in regulating epithelial plasticity.

The biological effects of BAP1 dysregulation are strongly context-dependent. In most cancer models, including uveal and cutaneous melanoma as well as renal cell carcinoma, BAP1 loss promotes stemness, activation of EMT programs, and aggressive tumor behavior [43–46]. However, a recent study in uveal melanoma reported the opposite effect, showing that BAP1 loss drives epithelial gene expression and promotes cell aggregation [47]. These apparently conflicting results highlight the complexity of BAP1 function, which likely depends on the cellular and epigenetic context. Our findings expand this framework to the trophoblast lineage, where sustained BAP1 expression similarly stabilizes epithelial features and impedes both invasive and syncytial differentiation. This emphasizes that timely BAP1 downregulation is essential for normal trophoblast plasticity and placental development.

By modulating epithelial traits, EMT and cell invasion, BAP1 provides a mechanistic bridge between placental development and oncogenic transformation, as comparable molecular networks govern trophoblast invasion and tumour metastasis [48]. Although a direct role for BAP1 in EMT regulation during development or tumorigenesis remains incompletely defined, reduced BAP1 expression in cancers with prominent EMT components, such as uveal melanoma, clear-cell renal cell carcinoma, gastric adenocarcinoma, colorectal cancer, and non-small-cell lung cancer, correlates with increased invasiveness and poorer prognosis [49–52]. These observations support a model in which low BAP1 levels facilitate EMT-driven malignancy. Nevertheless, the consequences of BAP1 loss vary across tissues. In renal tumor cells, for example, its inactivation promotes a mesenchymal-to-epithelial transition [53], underscoring the cell–type–specific nature of its regulatory functions. Further studies will be needed to delineate how BAP1 interacts with lineage-specific transcriptional and chromatin programs to fine-tune EMT regulation in different biological contexts.

Considering that BAP1 downregulation appears critical for trophoblast plasticity, we investigated how altering BAP1 expression, either through overexpression or knockdown, perturbs the differentiation of trophoblast lineages in vitro. In monolayer cultures, BAP1 overexpression impaired EVT differentiation by preventing the induction of key markers such as *HLA-G*, *ITGA5*, and *MMP2*, and by reducing MMP2 enzymatic activity, indicating diminished invasive capacity, a hallmark of EO-PE pathophysiology [10, 53–55]. Under STB differentiation conditions, BAP1-overexpressing cells exhibited reduced *CGB* expression and formed fewer and smaller syncytial clusters. In contrast, BAP1 knockdown did not significantly impact EVT or STB differentiation in 2D monolayers, suggesting that basal BAP1 expression is sufficient to sustain normal lineage specification in these simplified systems. Bulk transcriptomic and proteomic analyses of BAP1-overexpressing cells confirmed a failure to activate gene networks involved in glycoprotein biosynthesis, autophagy, and ER stress responses, processes essential for STB maturation and hormone production, and frequently altered in EO-PE placentas [32, 56, 57].

These functional defects were faithfully recapitulated in 3D trophoblast organoids, which model early villous architecture. Control organoids exhibited the expected organization, with a basal CTB layer surrounding a central STB core, whereas BAP1-overexpressing organoids showed reduced syncytialization, persistent expression of progenitor markers, and repression of endocrine differentiation pathways. Conversely, BAP1 knockdown produced an opposite yet complementary phenotype, characterized by excessive organoid growth and expansion of the CTB compartment, suggesting increased proliferative activity. Despite this hyperproliferation, BAP1-deficient organoids displayed defective STB formation, likely resulting from impaired spontaneous differentiation of the central cell population or disrupted signaling between CTB and emerging STB layers. This phenotype, where BAP1 depletion does not affect 2D differentiation but compromises STB generation specifically in 3D organoids, is consistent with previous observations [58], emphasizing the importance of spatial organization and intercellular communication in regulating trophoblast maturation, and highlighting the more physiological relevance of 3D organoid systems compared to conventional 2D cultures [59–62]. Together, these findings indicate that both excessive and insufficient BAP1 activity disturb the balance between trophoblast proliferation and differentiation, highlighting the need for precise temporal and spatial control of BAP1 during villous development. Transcriptomic and proteomic analyses of BAP1-overexpressing organoids further revealed enrichment of inflammatory and immune-related pathways, including interferon signaling, MHC class I peptide-loading, and cytokine activity, suggesting that BAP1 overexpression not only blocks differentiation but also promotes immune dysregulation. This phenotype mirrors the inflammatory milieu observed in EO-PE placentas, marked by excessive type I interferon activity, altered innate immune system, and aberrant maternal–fetal immune crosstalk [35, 63, 64]. These findings support a model in which BAP1 overexpression traps trophoblasts in an undifferentiated state, compromising both endocrine function and tissue remodeling capacity.

Mechanistically, BAP1 functions as the catalytic subunit of the PR-DUB complex, which removes monoubiquitin from histone H2A lysine 119 (H2AK119ub1), a modification associated with transcriptional repression [65]. PR-DUB function requires interaction with ASXL family proteins (ASXL1–3), which confer target specificity and modulate chromatin accessibility [66]. We show that BAP1 protein levels, and expression of *ASXL1* and *ASXL3* decrease, consistent with the progressive loss of progenitor identity. In contrast, BAP1, ASXL2, and ASXL3 are upregulated in placentas from EO-PE cases before 34 weeks of gestation, correlating with disease severity. Although *ASXL2* mRNA is significantly increased in EO-PE placentas, changes in BAP1 and ASXL3 are more evident at the protein level, consistent with evidence that PR-DUB activity is primarily regulated post-translationally through ASXL-dependent protein–protein

interactions that promote BAP1 stability and enzymatic activity [67–69], a mechanism we have previously shown to operate in trophoblast stem cells [24]. These findings suggest that dysregulation of PR-DUB activity may contribute to EO-PE by maintaining trophoblasts in a poorly invasive, poorly endocrine, progenitor-like state.

The upstream signals responsible for BAP1 and PR-DUB upregulation in early-onset preeclampsia (EO-PE) remain to be defined. Current evidence indicates that BAP1 expression and activity are dynamically modulated by cellular stress pathways, particularly hypoxia, whereas ER stress and interferon signaling are likely downstream consequences of excessive BAP1 activity rather than primary inducers. Under hypoxic conditions, BAP1 levels increase at both the mRNA and protein level, as demonstrated in nasopharyngeal carcinoma cells, where hypoxia-induced BAP1 enhances erastin-induced ferroptosis through histone H2A deubiquitination and repression of SLC7A11 [66, 70, 71]. BAP1 also interacts with and stabilizes HIF-1α, promoting its nuclear accumulation and transcriptional activity, whereas BAP1 loss reduces HIF-1α levels and impairs adaptation to oxygen deprivation [72]. These findings suggest that hypoxia is a physiological inducer of BAP1 expression, potentially linking placental oxygen tension to chromatin-based regulation of trophoblast differentiation.

In contrast, ER stress and interferon signaling appear to be modulated by BAP1 itself. BAP1 binds to the promoters of unfolded protein response (UPR) genes such as *ATF3* and *CHOP*, repressing their transcription during metabolic or ER stress [73]. This regulatory mechanism normally serves to fine-tune the UPR, preventing excessive activation and apoptosis. However, our findings indicate that excessive BAP1 expression in trophoblasts represses the UPR, thereby impairing the physiological ER stress response required for proper syncytialization [74]. In this context, BAP1 overexpression suppresses key UPR components and disrupts the adaptive stress signaling needed for the differentiation and fusion of villous cytotrophoblasts into syncytiotrophoblasts. This aberrant repression may contribute to defective syncytialization and placental dysfunction characteristic of EO-PE. Furthermore, BAP1 functions as an upstream activator of type I interferon pathways, inducing IFN-β expression and promoting STING and ISGF3 activation. Conversely, BAP1 loss weakens interferon signaling and reduces interferon-mediated tumor suppression [74]. These findings are consistent with our observation that BAP1-overexpressing trophoblast organoids display enhanced interferon signaling and a pro-inflammatory transcriptional phenotype that mirrors EO-PE. Together, these results suggest that aberrant BAP1 expression simultaneously suppresses adaptive ER stress responses and amplifies inflammatory interferon signaling, creating a dual imbalance that disrupts trophoblast homeostasis.

Collectively, this study identifies BAP1 as a key integrator of hypoxic, metabolic, and immune cues through chromatin-based regulation of gene expression. In the context of EO-PE, aberrant BAP1 activation may not only impair trophoblast differentiation but also exacerbate cellular stress and inflammatory responses, further compromising placental function. However, elevated BAP1 levels in vivo could initially arise as a secondary response to hypoxia, a hallmark of EO-PE placentas. Disentangling these causal relationships will require temporal analyses to determine how HIF-1α, UPR, and interferon pathways converge on BAP1 regulation in physiological versus pathological conditions.

In addition, our data implicate BAP1 in disrupting maternal–fetal immune tolerance. The suppression of HLA-G and concomitant activation of interferon-stimulated genes in BAP1-overexpressing trophoblasts mirror the immune alterations typical of EO-PE, where defective HLA-G expression and aberrant uterine NK cell function are hallmarks of disease.

Determining whether BAP1 dysregulation represents a primary pathogenic event or a downstream consequence of placental stress will be essential to elucidate the sequence of events leading to placental failure. Ultimately, identifying the upstream triggers and downstream consequences of aberrant PR-DUB activity may yield novel biomarkers for early EO-PE detection and inform molecular strategies to restore trophoblast homeostasis. Together, our findings position BAP1 as a central gatekeeper of trophoblast differentiation and placental health, offering a mechanistic framework for understanding how disruptions in chromatin regulation contribute to the pathogenesis of preeclampsia.

Limitations of the study

Although our data demonstrate that altered BAP1 levels disrupt trophoblast differentiation and recapitulate key molecular signatures of EO-PE, several limitations should be acknowledged. First, while we show that BAP1 and its cofactors are upregulated in EO-PE placentas, it remains unclear whether this reflects a primary pathogenic mechanism or a secondary adaptive response to placental stressors such as hypoxia, oxidative stress, or inflammation. Second, although we employ both BAP1 overexpression and knockdown models to interrogate the role of BAP1 in trophoblast biology, these perturbation systems may not fully capture the subtler and possibly heterogeneous dysregulation occurring in vivo. Future studies using patient-derived trophoblast organoids, primary cultures, or in vivo models will be essential to establish the causal hierarchy and physiological relevance of BAP1 dysregulation during placental development. Third, while our transcriptomic and proteomic datasets identify inflammatory and interferon-related pathways as major downstream consequences of BAP1 perturbation, we have not yet determined whether pharmacological or genetic inhibition of these pathways can restore normal trophoblast differentiation. Finally, although our study defines a global molecular landscape of BAP1-driven dysregulation, the specific mechanistic contributions of individual genes and proteins to EO-PE pathogenesis remain to be elucidated.

Addressing these limitations will be critical to delineate the upstream regulators and downstream effectors of BAP1 activity in the placenta and to evaluate its potential as a biomarker and therapeutic target for early-onset preeclampsia.

DATA AVAILABILITY

All data generated or analysed during this study are included in the manuscript and its supporting files. RNA-seq data have been deposited in the Gene Expression Omnibus (GEO) under accession number GSE311483, and mass spectrometry proteomics data have been deposited in the PRIDE partner repository via the ProteomeXchange Consortium under dataset identifier PXD071497. Raw data for all western blot experiments are included in the Supplementary file Original data. This study does not report original code. Any additional information required to reanalyse the data is available from the corresponding authors upon reasonable request.

REFERENCES

1. Knöfler M, Pollheimer J. Human placental trophoblast invasion and differentiation: a particular focus on Wnt signaling. Front Genet. 2013;4:60569.
2. Turco MY, Moffett A. Development of the human placenta. Development 2019;146. https://doi.org/10.1242/DEV.163428.
3. Hemberger M, Hanna CW, Dean W. Mechanisms of early placental development in mouse and humans. Nat Rev Genet. 2020;21:27–43.
4. Beristain AG, McNeill GL. Organoids in modeling human trophoblast development. Fertil Steril. 2025. https://doi.org/10.1016/J.FERTNSTERT.2025.10.004.
5. Okae H, Toh H, Sato T, Hiura H, Takahashi S, Shirane K, et al. Derivation of human trophoblast stem cells. Cell Stem Cell. 2018;22:50–63.e6.
6. Turco MY, Gardner L, Kay RG, Hamilton RS, Prater M, Hollinshead MS, et al. Trophoblast organoids as a model for maternal–fetal interactions during human placentation. Nature. 2018;564:263–81.

7. Haider S, Meinhardt G, Saleh L, Kunihs V, Gamperl M, Kaindl U, et al. Self-renewing trophoblast organoids recapitulate the developmental program of the early human placenta. Stem Cell Rep. 2018;11:537–51.
8. Romero R, Chaiworapongsa T. Preeclampsia: a link between trophoblast dysregulation and an antiangiogenic state. J Clin Investig. 2013;123:2775.
9. Natenzon A, McFadden P, DaSilva-Arnold SC, Zamudio S, Illsley NP. Diminished trophoblast differentiation in early-onset preeclampsia. Placenta. 2022;120:25–31.
10. Burton GJ, Redman CW, Roberts JM, Moffett A. Pre-eclampsia: pathophysiology and clinical implications. BMJ 2019;366. https://doi.org/10.1136/BMJ.L2381.
11. Wei XW, Zhang YC, Wu F, Tian FJ, Lin Y. The role of extravillous trophoblasts and uterine NK cells in vascular remodeling during pregnancy. Front Immunol. 2022;13:951482.
12. Langbein M, Strick R, Strissel PL, Vogt N, Parsch H, Beckmann MW, et al. Impaired cytotrophoblast cell-cell fusion is associated with reduced syncytin and increased apoptosis in patients with placental dysfunction. Mol Reprod Dev. 2008;75:175–83.
13. Dimitriadis E, Rolnik DL, Zhou W, Estrada-Gutierrez G, Koga K, Francisco RPV, et al. Pre-eclampsia. Nat Rev Dis Primers. 2023;9:1–22.
14. Yung HW, Atkinson D, Campion-Smith T, Olovsson M, Charnock-Jones DS, Burton GJ. Differential activation of placental unfolded protein response pathways implies heterogeneity in causation of early- and late-onset pre-eclampsia. J Pathol. 2014;234:262.
15. Tannetta D, Collett G, Vatish M, Redman C, Sargent I. Syncytiotrophoblast extracellular vesicles – circulating biopsies reflecting placental health. Placenta. 2017;52:134–8.
16. Collett GP, Redman CW, Sargent IL, Vatish M. Endoplasmic reticulum stress stimulates the release of extracellular vesicles carrying danger-associated molecular pattern (DAMP) molecules. Oncotarget. 2018;9:6707–17.
17. Chen Y, Huang Y, Jiang R, Teng Y. Syncytiotrophoblast-derived microparticle shedding in early-onset and late-onset severe pre-eclampsia. Int J Gynaecol Obstet. 2012;119:234–8.
18. Pillay P, Maharaj N, Moodley J, Mackraj I. Placental exosomes and pre-eclampsia: Maternal circulating levels in normal pregnancies and early and late onset pre-eclamptic pregnancies. Placenta. 2016;46:18–25.
19. McLaughlin K, Zhang J, Lye SJ, Parker JD, Kingdom JC. Phenotypes of pregnant women who subsequently develop hypertension in pregnancy. J Am Heart Assoc. 2018;7. https://doi.org/10.1161/JAHA.118.009595.
20. Perez-Garcia V, Fineberg E, Wilson R, Murray A, Mazzeo CI, Tudor C, et al. Placentation defects are highly prevalent in embryonic lethal mouse mutants. Nature. 2018;555:463–8.
21. Carbone M, Yang H, Pass HI, Krausz T, Testa JR, Gaudino G. BAP1 and cancer. Nat Rev Cancer. 2013;13:153–9.
22. Sahtoe DD, Van Dijk WJ, Ekkebus R, Ovaa H, Sixma TK. BAP1/ASXL1 recruitment and activation for H2A deubiquitination. Nat Commun. 2016;7:1–13.
23. Szczepanski AP, Wang L. Emerging multifaceted roles of BAP1 complexes in biological processes. Cell Death Discov. 2021;7:1–10.
24. Perez-Garcia V, Lea G, Lopez-Jimenez P, Okkenhaug H, Burton GJ, Moffett A, et al. BAP1/ASXL complex modulation regulates epithelial-mesenchymal transition during trophoblast differentiation and invasion. Elife. 2021;10:e63254.
25. Brown MA, Magee LA, Kenny LC, Karumanchi SA, McCarthy FP, Saito S, et al. Hypertensive disorders of pregnancy: ISSHP classification, diagnosis, and management recommendations for international practice. Hypertension. 2018;72:24–43.
26. Turco MY, Gardner L, Kay RG, Hamilton RS, Prater M, Hollinshead MS, et al. Trophoblast organoids as a model for maternal–fetal interactions during human placentation. Nature. 2018;564:263–7.
27. Branco MR, King M, Perez-Garcia V, Bogutz AB, Caley M, Fineberg E, et al. Maternal DNA methylation regulates early trophoblast development. Dev Cell. 2016;36:152–63.
28. Pérez-García V, Redondo-Muñoz J, Kumar A, Carrera AC. Cell activation-induced phosphoinositide 3-kinase alpha/beta dimerization regulates PTEN activity. Mol Cell Biol. 2014;34:3359–73.
29. Moggridge S, Sorensen PH, Morin GB, Hughes CS. Extending the compatibility of the SP3 paramagnetic bead processing approach for proteomics. J Proteome Res. 2018;17:1730–40.
30. Müller T, Kalxdorf M, Longuespée R, Kazdal DN, Stenzinger A, Krijgsveld J. Automated sample preparation with SP 3 for low-input clinical proteomics. Mol Syst Biol. 2020;16:e9111.
31. Dennis G, Sherman BT, Hosack DA, Yang J, Gao W, Lane HC, et al. DAVID: database for annotation, visualization, and integrated discovery. Genome Biol. 2003;4:1–1.
32. Álvarez-Sánchez A, Grinat J, Doria-Borrell P, Mellado-López M, Pedrera-Alcócer É, Malenchini M et al. The GPI-anchor biosynthesis pathway is critical for syncytiotrophoblast differentiation and placental development. Cell Mol Life Sci. 2024;81. https://doi.org/10.1007/S00018-024-05284-2.
33. Kim M, Jang YJ, Lee M, Guo Q, Son AJ, Kakkad NA et al. The transcriptional regulatory network modulating human trophoblast stem cells to extravillous trophoblast differentiation. Nat Commun 2024;15. https://doi.org/10.1038/S41467-024-45669-2.
34. Keenen MM, Yang L, Liang H, Farmer VJ, Worota RE, Singh R, et al. Comparative analysis of the syncytiotrophoblast in placenta tissue and trophoblast organoids using snRNA sequencing. Elife 2025;13. https://doi.org/10.7554/ELIFE.101170.
35. Harmon AC, Cornelius DC, Amaral LM, Faulkner JL, Cunningham MW, Wallace K, et al. The role of inflammation in the pathology of preeclampsia. Clin Sci. 2016;130:409.
36. Chung JY, Song Y, Wang Y, Magness RR, Zheng J. Differential expression of vascular endothelial growth factor (VEGF), endocrine gland derived-VEGF, and VEGF receptors in human placentas from normal and preeclamptic pregnancies. J Clin Endocrinol Metab. 2004;89:2484–90.
37. Zhang H, Xue L, Lv Y, Yu X, Zheng Y, Miao Z, et al. Integrated microarray analysis of key genes and a miRNA-mRNA regulatory network of early-onset preeclampsia. Mol Med Rep. 2020;22:4772–82.
38. Czikk MJ, Drewlo S, Baczyk D, Adamson SL, Kingdom J. Dual specificity phosphatase 9 (DUSP9) expression is down-regulated in the severe pre-eclamptic placenta. Placenta. 2013;34:174–81.
39. Zhang S, Zou Y, Tang X, Zhang Y, Yang N, Xu K, et al. Silencing of AFAP1-AS1 lncRNA impairs cell proliferation and migration by epigenetically promoting DUSP5 expression in pre-eclampsia. J Cell Biochem. 2021;122:1506–16.
40. Namlı Kalem M, Kalem Z, Yüce T, Soylemez F. ADAMTS 1, 4, 12, and 13 levels in maternal blood, cord blood, and placenta in preeclampsia. Hypertens Pregnancy. 2018;37:9–17.
41. Woods L, Perez-Garcia V, Hemberger M. Regulation of placental development and its impact on fetal growth-new insights from mouse models. Front Endocrinol. 2018;9. https://doi.org/10.3389/FENDO.2018.00570.
42. Artegiani B, van Voorthuijsen L, Lindeboom RGH, Seinstra D, Heo I, Tapia P, et al. Probing the tumor suppressor function of BAP1 in CRISPR-engineered human liver organoids. Cell Stem Cell. 2019;24:927–43.e6.
43. Matatall KA, Agapova OA, Onken MD, Worley LA, Bowcock AM, Harbour JW. BAP1 deficiency causes loss of melanocytic cell identity in uveal melanoma. BMC Cancer. 2013;13:371.
44. Peña-Llopis S, Vega-Rubín-De-Celis S, Liao A, Leng N, Pavía-Jiménez A, Wang S, et al. BAP1 loss defines a new class of renal cell carcinoma. Nat Genet. 2012;44:751.
45. Harbour JW, Onken MD, Roberson EDO, Duan S, Cao L, Worley LA, et al. Frequent mutation of BAP1 in metastasizing uveal melanomas. Science. 2010;330:1410.
46. Farag R, Jain F, Longakit AN, Luty A, Raamsdonk CD Van. BAP1-deficient human and mouse uveal melanomas up-regulate a shared EMT pathway. Preprint at https://doi.org/10.1101/2023.05.24.542173.
47. Baqai U, Purwin TJ, Bechtel N, Chua V, Han A, Hartsough EJ, et al. Multi-omics profiling shows BAP1 loss is associated with upregulated cell adhesion molecules in uveal melanoma. Mol Cancer Res. 2022;20:1260.
48. Doria-Borrell P, Pérez-García V. Understanding the intersection between placental development and cancer: lessons from the tumor suppressor BAP1. Commun Biol. 2024;7:1–12.
49. Tang J, Xi S, Wang G, Wang B, Yan S, Wu Y et al. Prognostic significance of BRCA1-associated protein 1 in colorectal cancer. Med Oncol. 2013;30. https://doi.org/10.1007/S12032-013-0541-8.
50. Fan LH, Tang LN, Yue L, Yang Y, Gao ZL, Shen Z. BAP1 is a good prognostic factor in advanced non-small cell lung cancer. Clin Investig Med. 2012;35. https://doi.org/10.25011/CIM.V35I4.17146.
51. Yan S, He F, Luo R, Wu H, Huang M, Huang C, et al. Decreased expression of BRCA1-associated protein 1 predicts unfavorable survival in gastric adenocarcinoma. Tumour Biol. 2016;37:6125–33.
52. Kalirai H, Dodson A, Faqir S, Damato BE, Coupland SE. Lack of BAP1 protein expression in uveal melanoma is associated with increased metastatic risk and has utility in routine prognostic testing. Br J Cancer. 2014;111:1373.
53. Chen P, Wang H, Zhang W, Chen Y, Lv Y, Wu D, et al. Loss of BAP1 results in growth inhibition and enhances mesenchymal–epithelial transition in kidney tumor cells. Mol Cell Proteom. 2019;18:1320–9.
54. Sosa SEY, Flores-Pliego A, Espejel-Núñez A, Medina-Bastidas D, Vadillo-Ortega F, Zaga-Clavellina V et al. New insights into the role of matrix metalloproteinases in preeclampsia. Int J Mol Sci 2017;18. https://doi.org/10.3390/IJMS18071448.
55. Huppertz B. The critical role of abnormal trophoblast development in the etiology of preeclampsia. Curr Pharm Biotechnol. 2018;19:771.
56. Carrasco-Wong I, Aguilera-Olguín M, Escalona-Rivano R, Chiarello DI, Barragán-Zúñiga LJ, Sosa-Macías M, et al. Syncytiotrophoblast stress in early-onset preeclampsia: the issues perpetuating the syndrome. Placenta. 2021;113:57–66.
57. Burton GJ, Yung HW. Endoplasmic reticulum stress in the pathogenesis of early-onset pre-eclampsia. Pregnancy Hypertens. 2011;1:72.

58. Lea G, Doria-Borrell P, Ferrero-Micó A, Varma A, Simon C, Anderson H, et al. Ectopic expression of DNMT3L in human trophoblast stem cells restores features of the placental methylome. Cell Stem Cell. 2025;32:276–92.e9.
59. Karvas RM, Khan SA, Verma S, Yin Y, Kulkarni D, Dong C, et al. Stem-cell-derived trophoblast organoids model human placental development and susceptibility to emerging pathogens. Cell Stem Cell. 2022;29:810.
60. Hori T, Okae H, Shibata S, Kobayashi N, Kobayashi EH, Oike A, et al. Trophoblast stem cell-based organoid models of the human placental barrier. Nat Commun. 2024;15:1–15.
61. Yang L, Liang P, Yang H, Coyne CB. Trophoblast organoids with physiological polarity model placental structure and function. J Cell Sci 2024;137. https://doi.org/10.1242/JCS.261528/VIDEO-4.
62. Sheridan MA, Zhao X, Fernando RC, Gardner L, Pérez-García V, Li Q, et al. Characterization of primary models of human trophoblast. Development. 2021;148:dev199749.
63. Broekhuizen M, Hitzerd E, van den Bosch TPP, Dumas J, Verdijk RM, van Rijn BB, et al. The placental innate immune system is altered in early-onset preeclampsia, but not in late-onset preeclampsia. Front Immunol. 2021;12:780043.
64. Ding J, Maxwell A, Adzibolosu N, Hu A, You Y, Liao A, et al. Mechanisms of immune regulation by the placenta: role of type I interferon and interferon-stimulated genes signaling during pregnancy. Immunol Rev. 2022;308:9–24.
65. Tamburri S, Lavarone E, Fernández-Pérez D, Conway E, Zanotti M, Manganaro D, et al. Histone H2AK119 mono-ubiquitination is essential for polycomb-mediated transcriptional repression. Mol Cell. 2020;77:840–56.e5.
66. Kwon J, Lee D, Lee SA. BAP1 as a guardian of genome stability: implications in human cancer. Exp Mol Med. 2023;55:745–54.
67. Cai W, Wu S, Lin Z, Ming X, Yang X, Yang M, et al. Hypoxia-induced BAP1 enhances erastin-induced ferroptosis in nasopharyngeal carcinoma by stabilizing H2A. Cancer Cell Int. 2024;24:307.
68. Zhang Y, Shi J, Liu X, Feng L, Gong Z, Koppula P, et al. BAP1 links metabolic regulation of ferroptosis to tumour suppression. Nat Cell Biol. 2018;20:1181–92.
69. Bononi A, Wang Q, Zolondick AA, Bai F, Steele-Tanji M, Suarez JS, et al. BAP1 is a novel regulator of HIF-1α. Proc Natl Acad Sci USA 2023;120. https://doi.org/10.1073/PNAS.2217840120.
70. Dai F, Lee H, Zhang Y, Zhuang L, Yao H, Xi Y, et al. BAP1 inhibits the ER stress gene regulatory network and modulates metabolic stress response. Proc Natl Acad Sci USA 2017;114:3192–7.
71. Bastida-Ruiz D, Yart L, Wuillemin C, Ribaux P, Morris N, Epiney M, et al. The fine-tuning of endoplasmic reticulum stress response and autophagy activation during trophoblast syncytialization. Cell Death Dis. 2019;10:1–15.
72. Langbein LE, El Hajjar R, He S, Sementino E, Zhong Z, Jiang W, et al. BAP1 maintains HIF-dependent interferon beta induction to suppress tumor growth in clear cell renal cell carcinoma. Cancer Lett. 2022;547:215885.
73. Boulanger H, Bounan S, Mahdhi A, Drouin D, Ahriz-Saksi S, Guimiot F, et al. Immunologic aspects of preeclampsia. AJOG Glob Rep. 2024;4. https://doi.org/10.1016/j.xagr.2024.100321.
74. Aisagbonhi O, Morris GP. Human Leukocyte Antigens in Pregnancy and Pre-eclampsia. Front Genet. 2022;13. https://doi.org/10.3389/FGENE.2022.884275.

ACKNOWLEDGEMENTS

We thank Dr. Hiroaki Okae and Dr. Takahiro Arima for generously providing the hTSC cell lines used in this study. We are also deeply grateful to the donors whose contributions made this research possible. We acknowledge the support of the Advanced Light Microscopy Facility at the Centro de Biología Molecular "Severo Ochoa" (Madrid, Spain). This work was funded by the Ministerio de Ciencia e Innovación, Agencia Estatal de Investigación (MICIU/AEI/10.13039/501100011033), under grant numbers PID2020-114459RA-I00, PID2023-148535OB-I00, and CNS2022-135933, as well as by the Fundación Ramón Areces. AF-M is supported by a PhD fellowship from the Asociación Española Contra el Cáncer (AECC) – Comunitat Valenciana. LY was supported by the BITRECS fellowship programme ("Biomedicine International Training Research Programme for Excellent Clinician-Scientist") at Hospital Clínic de Barcelona, funded by the "la Caixa" Foundation (grant code LCF/PR/SP23/52950012). FC received support from Hospital Clínic de Barcelona (Intensificació Interna) and the Fundació Jesús Serra of the Grup Catalana Occident.

AUTHOR CONTRIBUTIONS

VP-G conceptualized the study. PD-B, AF-M, SN-S, MM-L, JG, and CM performed experiments and generated data for this study. LY, CM, FC, and TK undertook human placenta sample isolation. PD-B and SN-S performed bioinformatics analyses. VP-G drafted the manuscript, with input from all authors.

COMPETING INTERESTS

The authors declare no competing interests.

ADDITIONAL INFORMATION

Supplementary information The online version contains supplementary material available at https://doi.org/10.1038/s41419-026-08650-z.

Correspondence and requests for materials should be addressed to Vicente Pérez-García.

Reprints and permission information is available at http://www.nature.com/reprints

Publisher's note Springer Nature remains neutral with regard to jurisdictional claims in published maps and institutional affiliations.

Open Access This article is licensed under a Creative Commons Attribution 4.0 International License, which permits use, sharing, adaptation, distribution and reproduction in any medium or format, as long as you give appropriate credit to the original author(s) and the source, provide a link to the Creative Commons licence, and indicate if changes were made. The images or other third party material in this article are included in the article's Creative Commons licence, unless indicated otherwise in a credit line to the material. If material is not included in the article's Creative Commons licence and your intended use is not permitted by statutory regulation or exceeds the permitted use, you will need to obtain permission directly from the copyright holder. To view a copy of this licence, visit http://creativecommons.org/licenses/by/4.0/.

© The Author(s) 2026